International Journal of Control

ISSN: 0020-7179 (Print) 1366-5820 (Online) Journal homepage: https://www.tandfonline.com/loi/tcon20

Estimating parameters with pre-specified accuracies in distributed parameter systems using optimal experiment design

M. G. Potters, X. Bombois, M. Mansoori & Paul M. J. Van den Hof

To cite this article: M. G. Potters, X. Bombois, M. Mansoori & Paul M. J. Van den Hof (2016) Estimating parameters with pre-specified accuracies in distributed parameter systems using optimal experiment design, International Journal of Control, 89:8, 1533-1553, DOI: 10.1080/00207179.2016.1138143

To link to this article: https://doi.org/10.1080/00207179.2016.1138143

INTERNATIONAL JOURNAL OF CONTROL, 2016
VOL. 89, NO. 8, 1533–1553
http://dx.doi.org/10.1080/00207179.2016.1138143

Taylor & Francis
Taylor & Francis Group

Estimating parameters with pre-specified accuracies in distributed parameter systems using optimal experiment design

M. G. Potters[a], X. Bombois[b], M. Mansoori[a,c] and Paul M. J. Van den Hof[d]

[a]Delft Center for Systems and Control, Delft University of Technology, Delft, The Netherlands; [b]Laboratoire Ampère UMR CNRS 5005, Ecole Centrale de Lyon, Ecully Cedex, France; [c]Department of Chemical and Petroleum Engineering, Sharif University of TechnologyTehran, Iran; [d]Department of Electrical Engineering, Eindhoven University of Technology, Eindhoven, The Netherlands

ABSTRACT

Estimation of physical parameters in dynamical systems driven by linear partial differential equations is an important problem. In this paper, we introduce the least costly experiment design framework for these systems. It enables parameter estimation with an accuracy that is specified by the experimenter prior to the identification experiment, while at the same time minimising the cost of the experiment. We show how to adapt the classical framework for these systems and take into account scaling and stability issues. We also introduce a progressive subdivision algorithm that further generalises the experiment design framework in the sense that it returns the lowest cost by finding the optimal input signal, and optimal sensor and actuator locations. Our methodology is then applied to a relevant problem in heat transfer studies: estimation of conductivity and diffusivity parameters in front-face experiments. We find good correspondence between numerical and theoretical results.

ARTICLE HISTORY
Received 10 April 2015
Accepted 30 December 2015

KEYWORDS
Distributed systems; optimal experiment design; physical systems; identification; accurate; simulation; optimal actuator and sensor locations

1. Introduction

Accurate estimation of key physical parameters in a system is an important problem. We mention some examples: a material can be characterised by its conductivity and diffusivity constants in heat transfer studies (Gabano & Poinot, 2009), realistic groundwater contamination simulations require accurate estimates of diffusivity and advection constants (Wagner & Harvey, 1997; Yeh, 1986), permeability and porosity of rock aid in oil extraction from subsurface reservoirs (Mansoori, Van den Hof, Janssen, & Rashtchian, 2014), etc. In this context, we consider in this paper the problem of optimally designing the identification experiment leading to the estimates of these physical parameters. More particularly, we design the least-intrusive excitation signal that nevertheless leads to parameter estimates with variances that do not exceed certain given (user-chosen) limits. Physical systems can have different structures. In this paper, we are particularly interested in those systems that can be described by linear partial differential equations (PDEs) with spatially independent coefficients.

Such systems are characterised by equations that not only contain time derivatives but also spatial ones. In the System Identification literature, they are usually referred to as distributed systems. The phenomena described by such equations are quite pervasive in the physical world (convection, diffusion, diffusion–advection–reaction, wave phenomena). Consequently, it is of importance to be able to design experiments that will allow identification of physical parameters in those systems in an accurate manner. Unfortunately, as their dynamics are described by PDEs, the classical optimal experiment design[1] techniques that have been developed for systems described by ordinary differential equations (ODEs) cannot be directly applied (see e.g. Bombois, Scorletti, Van den Hof, & Hildebrand, 2006; Jansson & Hjalmarsson, 2005). The classical approaches will, therefore, have to be adapted. This is one of the contributions of the present paper. Moreover, the particular structure of the systems described by PDEs allows us to analyse an additional design aspect that is usually not considered in optimal (least costly) experiment design: the location of the actuator that will excite the system and the location of the sensor that will measure the output of the system for the purpose of identification. Indeed, as mentioned in the recent book of Uciński (2004), most literature on optimal sensor and actuator location in distributed systems deals with state estimation, but few works actually address parameter identification. Yet, finding such locations can greatly improve the accuracy of the estimates, as shown in Rensfelt, Mousavi, Mossberg, and Söderström (2008). This paper addresses the problem of finding the

CONTACT M. G. Potters m.g.potters@tudelft.nl

optimal sensor and actuator locations *as well as* finding the optimal spectrum of the input signal.

Before addressing optimal experiment design for systems described by PDEs, let us first discuss how we will perform the identification of the physical parameter vector $\boldsymbol{\theta}_0$ of such a system. Like all physical systems, the systems described by PDEs are continuous-time systems. Since we assume linearity, the relation between the continuous-time input and output is given by a continuous-time transfer function $G(s, \boldsymbol{\theta}_0)$ in the Laplace variable s ($\boldsymbol{\theta}_0$ appears explicitly in $G(s, \boldsymbol{\theta}_0)$). However, for systems described by PDEs, this continuous-time transfer function is not rational in s (it can be, for example, $G(s) = \cosh(\sqrt{s})$). A closed-form expression of $G(s, \boldsymbol{\theta}_0)$ can be derived if the PDE is analytically tractable, although this is in general not possible for complicated (high-order, coupled) systems. Because the data that will be used for the identification are discrete, we need a discrete-time representation of $G(s, \boldsymbol{\theta}_0)$ that is also explicit in $\boldsymbol{\theta}_0$. However, such a representation does not exist in practice (it would be of infinite order). To circumvent this problem, spatio-temporal discretisation is generally applied and yields a finite-order approximation $G(z, \boldsymbol{\theta}_0)$ of the discrete-time transfer function between the discrete-time input and output data. The approximation consists of dividing the spatial dimension into a finite number of intervals in which the states of the systems are supposed constant. The order of $G(z, \boldsymbol{\theta}_0)$ is then related to the number of intervals in the grid. This spatio-temporal discretisation yields a transfer function that is still explicit in $\boldsymbol{\theta}_0$. Different discretisation schemes exist. In this paper, we propose to use the Crank–Nicolson stencil, which is unconditionally stable, and also ensures that the finite-order approximation $G(z, \boldsymbol{\theta}_0)$ is stable. Once we have the description of the system in the form of the transfer function $G(z, \boldsymbol{\theta}_0)$, it is straightforward to use the input–output data to identify the parameter vector $\boldsymbol{\theta}_0$ using prediction-error techniques.

A second method to simulate/identify the system explicit in $\boldsymbol{\theta}$ exists. When the PDE is analytically tractable we can make use of the linearity of the system to calculate the system response (Ljung, 1999). However, this method is only applicable for an input signal that is a superposition of sines.

These two approaches are not the only ones possible to identify the physical parameter vector $\boldsymbol{\theta}_0$. Rational or fractional black-box model can also be first identified and then the physical parameters be deduced from the parameters of the black-box model (see, for instance, Aoun, Malti, Levron, & Oustaloup, 2004; Gabano & Poinot, 2001; Point & Trigeassou, 2003; Point, Trigeassou, & Lin, 2002). However, these approaches require models with many parameters that are implicitly coupled to the physical ones. As such, the identification procedure will be numerically heavy. If the continuous-time transfer function $G(s, \boldsymbol{\theta}_0)$ can be expressed in closed form, frequency-domain approaches can also be used to identify $\boldsymbol{\theta}_0$ from the collected data (see, for instance, Pintelon, Schoukens, Pauwels, & van Gheem, 2005). Recently, a nice instrumental variable method has also been proposed in Schorsch, Garnier, Gilson, and Young (2013). However, we have chosen the approach via $G(z, \boldsymbol{\theta}_0)$ since it is the most general, the most straightforward and necessary for optimal experiment design.

Now we have defined our identification method and we have an expression of $G(z, \boldsymbol{\theta}_0)$ (which in general is also a function of the sensor and actuator locations, or other design variables), we can use classical optimal experiment design techniques (Bombois et al., 2006; Jansson & Hjalmarsson, 2005) to optimally design the input signal for the identification of the physical parameter vector $\boldsymbol{\theta}_0$. The to-be-designed optimal signal has to be parameterised. Generally, it is parameterised as a superposition of sinusoids (e.g. a multi-sine) or a filtered white noise. These parameterisations make the optimal experiment design problem convex and finite dimensional. The transfer function $G(z, \boldsymbol{\theta}_0)$ being generally of large order, it is more practical to parameterise the to-be-designed optimal input signal as a multi-sine (with fixed frequencies, but free amplitudes). Indeed, in this particular case, only the frequency response of the gradient of $G(z, \boldsymbol{\theta}_0)$ with respect to $\boldsymbol{\theta}_0$ is required for optimal experiment design. (Note that to calculate this gradient, we indeed need $G(z, \boldsymbol{\theta}_0)$ to be explicit in $\boldsymbol{\theta}_0$.) In the case where a closed-form expression of $G(s, \boldsymbol{\theta}_0)$ exists, we also propose a simpler approach. We indeed use the property that the frequency responses of $G(s, \boldsymbol{\theta}_0)$ and of $G(z, \boldsymbol{\theta}_0)$ are equal in the limit when the sampling time goes to zero, and almost equal for small sampling times. The frequency response of the gradient of the usually simpler continuous-time transfer function $G(s, \boldsymbol{\theta}_0)$ can then be used in the optimal experiment design procedure. The approach above can be applied for each sensor/actuator location in a very easy way and the optimal experiments for each location can be compared, allowing to determine the optimal locations.

We apply our methodology to one-dimensional (1D), second-order linear PDEs with spatially independent coefficients. Diffusion–advection–reaction processes in real life can be modelled with this family of equations. We stress that our methodology is applicable to higher dimensional, higher order PDE systems with different boundary conditions (as long as a discrete-time transfer function between input and output can be determined). We introduce and scale the continuous-time physical models in Sections 2 and 2.1. The unscaled

physical model represents the (continuous-time) true system which will be used to identify the physical parameters $\boldsymbol{\theta}_0$ with the use of our optimal input signal. The scaled model will be used for optimal input signal design and in the identification procedure. This procedure, together with the generation of discrete-time input and output signals, is explained in Section 3. The identification procedure requires simulation of the output as a function of $\boldsymbol{\theta}$ and is introduced in Section 3.2.1. The experiment design framework is explained in Section 4 and shows how to generate the optimal input signal for given choice of sensor and actuator locations. We generalise the OED framework in Section 4.2, where now also optimal sensor and actuator locations are computed. In Section 5, we apply our methodology to a diffusion process in which two material properties are identified with a front-face experiment.

2. Diffusion–advection–reaction processes

The diffusion–advection–reaction equation typically contains only a few key physical parameters, the most important one being the so-called diffusivity parameter, i.e. the hydraulic diffusivity parameter in flow through porous media, the conductivity coefficient in conductive heat transfer, the diffusion parameter in mass transfer, etc. Although this lumped parameter is a function of microscopic properties of the system, it characterises the observed macroscopic dynamic behaviour of the system effectively. Hence, using macroscopic measurements of the system, it is possible to estimate such parameters. We shall use the family of diffusion–advection–reaction processes as a showcase of our methodology, but we remind the reader that it is applicable to higher order linear PDE processes. Furthermore, we make a particular choice of boundary conditions, but many others exist that can also be applied within our framework. However, it is important to note that we restrict attention to systems with physical parameters that are not spatially dependent.

Diffusion–advection–reaction processes are described by the following family of second-order linear PDEs: [2]

$$\frac{\partial f(x,t)}{\partial t} = \theta_1 \frac{\partial^2 f(x,t)}{\partial x^2} + \theta_2 \frac{\partial f(x,t)}{\partial x} + \theta_3 f(x,t), \tag{1}$$

where $f(x, t)$ represents a macroscopic physical quantity at continuous time t and continuous position x. The coefficients $\theta_1 > 0, \theta_2, \theta_3$ are physical parameters. The spatial domain is defined by $\mathcal{D} = [0, L]$, where L is the total considered length. We assume zero initial conditions at $t = 0$. The boundary conditions are

$$\begin{aligned} -\theta_4 \left.\frac{\partial f(x,t)}{\partial x}\right|_{x=x_u} &= u(t),\ y_{\mathrm{nf}}(t) \\ &= f(x_y,t) \ \text{ and } \ f(L,t) = 0\,\forall t. \end{aligned} \tag{2}$$

The physical parameters are collected in the vector $\boldsymbol{\theta} = (\theta_1, \theta_2, \theta_3, \theta_4)^T$. The first boundary condition in (2) is of the second kind, known as the Neumann boundary condition. It expresses the flow rate across the boundary at position $x = x_u$ induced by the influx $u(t)$. We define $u(t)$ as the user-imposed (known) input signal to the physical system and, therefore, call $x_u \in \mathcal{D}$ the input location. The second boundary condition defines the noise-free output $y_{\mathrm{nf}}(t)$ being equal to the physical quantity $f(x, t)$ at output measurement location $x = x_y \in \mathcal{D}$. We thus consider a single-input, single-output system. The third boundary condition states that the physical quantity $f(x, t)$ at location $x = L$ is equal to zero at all times.

Definition 2.1: The data-generating system is defined by Equations (1) and (2) and setting $\boldsymbol{\theta} = \boldsymbol{\theta}_0$, where $\boldsymbol{\theta}_0$ are the true physical parameter values.

If the data-generating system is analytically tractable, then a Laplace transform of Equations (1) and (2) allows us to relate the input $u(t)$ and output $y_{\mathrm{nf}}(t)$ of the data-generating system through

$$Y_{\mathrm{nf}}(s) = G_{x_u,x_y}(s, \boldsymbol{\theta}_0) U(s), \tag{3}$$

where s is the Laplace variable, $Y_{\mathrm{nf}}(s) = \mathcal{L}\left\{f(x_y, t)\right\}$ the Laplace transform of $y_{\mathrm{nf}}(t)$, $U(s) = \mathcal{L}\{u(t)\}$ the Laplace transform of $u(t)$, and $G_{x_u,x_y}(s, \boldsymbol{\theta}_0)$ is defined as their transfer function. The subscripts x_u, x_y indicate that the transfer function depends on the input and output locations. Hence, the above relation shows that the physical system may be interpreted as a linear, time-invariant system defined through input $U(s)$, output $Y_{\mathrm{nf}}(s)$ and transfer function $G_{x_u,x_y}(s, \boldsymbol{\theta}_0)$. As mentioned in Section 1, this transfer function will be irrational and of infinite order in s.

2.1 Non-dimensionalisation

An inherent feature of physical systems is the order-of-magnitude difference between the input and output variables and the physical parameters. Numerical simulation of the unscaled system (1)-(2) is prone to numerical difficulties, especially when considering the optimal experiment design algorithm, which uses a covariance matrix expression of the parameters. Without scaling, this matrix is usually ill-conditioned and consequently the algorithm

cannot usually find a solution to the optimisation problem.

To avoid these difficulties, we non-dimensionalise Equations (1) and (2) as follows:

(1) Scale parameter vector $\boldsymbol{\theta}$: $\tilde{\boldsymbol{\theta}} = \boldsymbol{\Theta}_s^{-1}\boldsymbol{\theta}$, where $\boldsymbol{\Theta}_s = \text{diag}(\theta_{s,1}, \ldots, \theta_{s,4})$ is a diagonal matrix containing the scaling factors for each element θ_i in the vector $\boldsymbol{\theta}$,

(2) Non-dimensionalise all variables:

$$\tilde{f} = \frac{f}{f_s}, \quad \tilde{u} = \frac{u}{u_s}, \quad \tilde{x} = \frac{x}{x_s}, \quad \tilde{t} = \frac{t}{t_s}, \tag{4}$$

where f_s, u_s, x_s, and t_s are as-of-yet undecided scaling values,

(3) Rewrite Equations (1) and (2) in terms of the non-dimensional parameters and variables defined in steps (1) and (2):

$$\frac{\partial \tilde{f}(\tilde{x},\tilde{t})}{\partial \tilde{t}} = \tilde{\theta}_1 \frac{\theta_{s,1} t_s}{x_s^2} \frac{\partial^2 \tilde{f}(\tilde{x},\tilde{t})}{\partial \tilde{x}^2} + \tilde{\theta}_2 \frac{\theta_{s,2} t_s}{x_s} \frac{\partial \tilde{f}(\tilde{x},\tilde{t})}{\partial \tilde{x}} + \tilde{\theta}_3 \theta_{s,3} t_s \tilde{f}(\tilde{x},\tilde{t}), \tag{5}$$

with boundary conditions

$$-\tilde{\theta}_4 \frac{\theta_{s,4} f_s}{u_s x_s} \frac{\partial \tilde{f}(\tilde{x},\tilde{t})}{\partial \tilde{x}} \Big|_{\tilde{x}=\tilde{x}_u} = \tilde{u}(\tilde{t}), \ \tilde{y}_{\text{nf}}(\tilde{t}) = \tilde{f}(\tilde{x}_y,\tilde{t}) \text{ and } \tilde{f}\left(\frac{L}{x_s},\tilde{t}\right) = 0 \ \forall \tilde{t}, \tag{6}$$

(4) Select f_s, u_s, x_s and t_s such that as many as possible terms in Equations (5) and (6) are solely a function of $\tilde{\boldsymbol{\theta}}$, and therefore of $O(1)$. The selection is not unique. One possible choice is to freely choose f_s and determine x_s, t_s and u_s as the solution of the following three equations: $t_s = x_s^2/\theta_{s,1}$, $x_s = \theta_{s,2} t_s$ and $u_s = \theta_{s,4} f_s / x_s$. This leads to $x_s = \theta_{s,1}/\theta_{s,2}$, $t_s = \theta_{s,1}/\theta_{s,2}^2$ and $u_s = \theta_{s,4}\theta_{s,2} f_s/\theta_{s,1}$. If some $\tilde{\theta}_i$ are zero, more freedom is available.

Step (1) ensures that the dimensionless parameters are $O(1)$ (i.e. have a value in between [0, 1]), a necessary step in order to apply experiment design. Although we do not know the actual values of $\boldsymbol{\theta}_0$, we do know their order of magnitude. Consequently, each element in the scaled vector $\boldsymbol{\theta}$ can be made of order one. Step (4) simplifies the non-dimensional system and shows which processes (i.e. diffusion, advection or reaction) are dominant.[3] Substitution of $\boldsymbol{\theta} = \boldsymbol{\theta}_0$ in step (1) and following the scaling procedure then defines the scaled equivalent of the *data − generating system* as detailed in Definition 2.1.

The relation between the scaled output $\tilde{y}_{\text{nf}}$ and scaled input $\tilde{u}(\tilde{t})$ for the family of scaled physical systems reads

$$\tilde{Y}_{\text{nf}}(\tilde{s}) = \tilde{G}_{\tilde{x}_u,\tilde{x}_y}(\tilde{s},\tilde{\boldsymbol{\theta}})\tilde{U}(\tilde{s}), \tag{7}$$

where now $\tilde{Y}_{\text{nf}}(\tilde{s}) = \mathcal{L}\{\tilde{f}(\tilde{x}_y,\tilde{t})\}$, $\tilde{U}(\tilde{s}) = \mathcal{L}\left\{\tilde{u}(\tilde{t})\right\}$ and $\tilde{s} = s\,t_s$. This equation is the scaled equivalent of Equation (3) for $\tilde{\boldsymbol{\theta}} = \tilde{\boldsymbol{\theta}}_0 \equiv \boldsymbol{\Theta}_s^{-1}\boldsymbol{\theta}_0$.

3. Data generation and the identification procedure

3.1 Data generation

In the previous sections, we have defined the continuous-time *data − generating system* (see Definition 2.1). This system represents the true physical process of which we want to identify the physical parameters $\boldsymbol{\theta}_0$. To accomplish this, we apply a continuous time (analogue) input signal $u(t)$ to the data-generating system leading to the continuous noise-free output $y_{\text{nf}}(t)$. This output is measured with a sampling time T_s and corrupted by zero-mean white noise with variance σ_e^2. The measurements are thus given by

$$y_D[n] \equiv y_{\text{nf}}(nT_s) + e(nT_s). \tag{8}$$

We will generally consider sinusoidal input signals (and thus sinusoidal output signals). The sampling time is generally chosen in such a way that the Nyquist frequency π/T_s is a decade above all dynamics of the system (i.e. the system's bandwidth). We shall denote $Z_N = \{u_D[n], y_D[n]\}_{n=1,\ldots,N}$ as the set containing the sampled input and output data. The values u_D will not always be used in the identification procedure.

3.2 Identification procedure

We identify the physical parameter vectors $\boldsymbol{\theta}_0$ using the collected data. First, we scale the data-set Z_N using Equation (4) to $\tilde{Z}_N = \left\{\frac{u_D[j]}{u_s}, \frac{y_D[j]}{f_s}\right\}$, where now our data points are shifted in time to $\tilde{t} = jT_s/t_s$. The scaled continuous-time noise-free output $\tilde{y}_{\text{nf}}(\tilde{t})$ is depicted in the right plot in Figure 1 in black, whereas the scaled measured data points $y_D[j]/f_s$ are shown in red. Observe that due to the time scaling, the temporal distance between the data points has become $\tilde{T}_s = T_s/t_s$.

The scaled true physical parameter $\tilde{\boldsymbol{\theta}}_0 = \boldsymbol{\Theta}_s^{-1}\boldsymbol{\theta}_0$ can now be estimated with the least-squares method:

$$\hat{\tilde{\boldsymbol{\theta}}}_N = \arg\min_{\tilde{\boldsymbol{\theta}}} \frac{1}{N}\sum_{j=1}^{N}\left[\frac{y_D[j]}{f_s} - \tilde{y}_{\text{sim}}(\tilde{\boldsymbol{\theta}})[j]\right]^2, \tag{9}$$

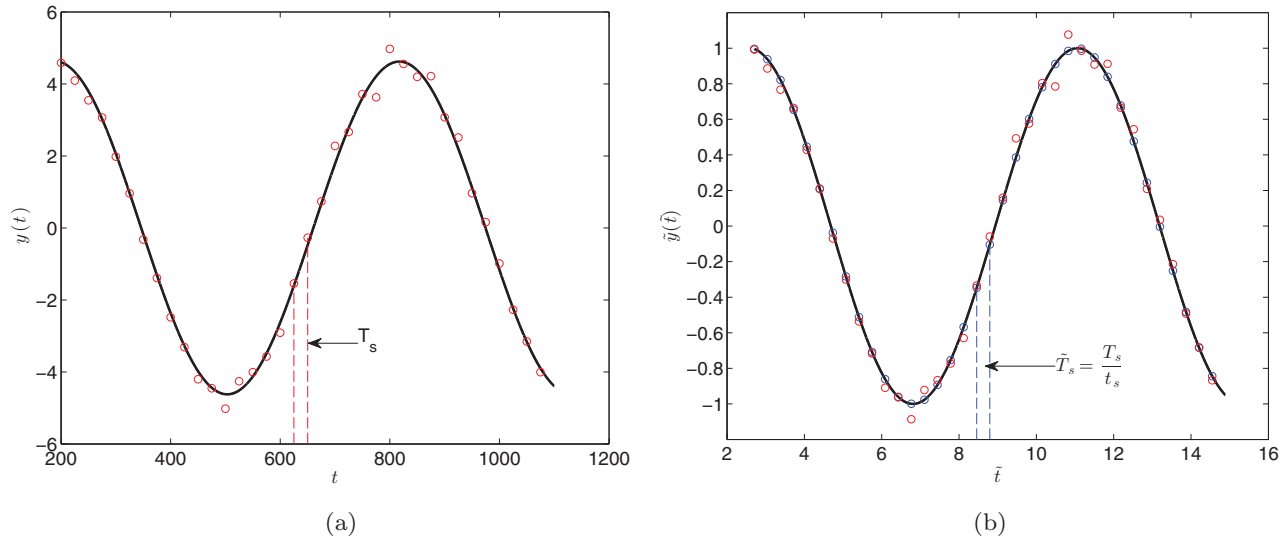

Figure 1. Left: unscaled continuous-time output signal as a function of time (black) and the noise-corrupted measured discrete-time signal (red). Right: scaled continuous-time output (black), scaled noise-corrupted measured discrete-time signal (red), and scaled simulated output data (blue). T_s is the unscaled sampling time, t_s the time scaling and $\tilde{T}_s$ the scaled sampling time.

where $\tilde{y}_{\text{sim}}(\tilde{\boldsymbol{\theta}})[j]$ is the sampled version of the output $\tilde{y}_{\text{nf}}(\tilde{t}$ of the scaled system (5) and (6) for an arbitrary $\tilde{\boldsymbol{\theta}}$ and $y_D[j]/f_s$ is the scaled measured output from the data-generating system. The unscaled estimate can then easily be retrieved by calculating $\hat{\boldsymbol{\theta}}_N = \boldsymbol{\Theta}_s \hat{\tilde{\boldsymbol{\theta}}}_N$ (cf Equation (4)). It is apparent from Equation (9) that we require an expression for $\tilde{y}_{\text{sim}}(\tilde{\boldsymbol{\theta}})$ for estimation.

To simulate the noise-free scaled output $\tilde{y}_{\text{nf}}(\tilde{t})$ (cf Equation (6)) for arbitrary values of the physical parameters $\tilde{\boldsymbol{\theta}}$, we can use two methods.

(1) If the input signal is chosen to be a superposition of sinusoids, its scaled form being

$$\tilde{u}(\tilde{t}) = \sum_{l=1}^{Q} \tilde{A}_l \sin(\omega_l t_s \tilde{t}) = \sum_{l=1}^{Q} \tilde{A}_l \sin(\tilde{\omega}_l \tilde{t}), \tag{10}$$

where $\tilde{\omega}_l = \omega_l t_s$ and $\tilde{A}_l = A_l/u_s$, then the continuous-time simulated output reads (Ljung, 1999)

$$\tilde{y}_{\text{sim}}(\tilde{\boldsymbol{\theta}}, t) = \sum_{l=1}^{Q} \tilde{A}_l |\tilde{G}_{\tilde{x}_u,\tilde{x}_y}(i\tilde{\omega}_l, \tilde{\boldsymbol{\theta}})| \sin(\tilde{\omega}_l \tilde{t} + \alpha_l), \tag{11}$$

where $\alpha_l = \angle \tilde{G}_{\tilde{x}_u,\tilde{x}_y}(i\tilde{\omega}_l, \tilde{\boldsymbol{\theta}})$, the transfer function $\tilde{G}_{\tilde{x}_u,\tilde{x}_y}$ defined in Equation (7) and Q a positive integer. Sampling this signal with the scaled sampling time T_s/t_s generates $\tilde{y}_{\text{sim}}(\tilde{\boldsymbol{\theta}})[j]$ that is used in Equation (9).

(2) Discretise Equations (5) and (6) using a finite-difference method which is detailed in Section 3.2.1. This method discretises time and space at an interval of $\Delta\tilde{t}$ and $\Delta\tilde{x}$, respectively. The constant $\Delta\tilde{t}$ is called the time integration step. Let us choose $\Delta\tilde{t} = \tilde{T}_s = T_s/t_s$. Then, we can apply an arbitrary input signal $u(t)$ to the data-generating system. The sampled scaled input $\tilde{u}_D$ from $\tilde{Z}_N$ can then be used to simulate the output $\tilde{y}_{\text{sim}}(\tilde{\boldsymbol{\theta}})[j]$ of which the samples are separated at an interval of T_s/t_s. The simulated points are shown in blue for $\tilde{\boldsymbol{\theta}} = \boldsymbol{\Theta}_s^{-1}\boldsymbol{\theta}_0$ and as can be observed, they occur at the same time instance as the scaled measured output data from $\tilde{Z}_N$.

Method (1) can be only be used for sinusoidal input signals and if a closed-form expression of $\tilde{G}_{\tilde{x}_u,\tilde{x}_y}$ exists. Method (2) is the most generic one as it can be used when the $\tilde{G}_{\tilde{x}_u,\tilde{x}_y}$ does not have a closed-form expression and/or the input signal is not a sum of sinusoids. From now on, we will consider method (2). We now show how to generate $\tilde{y}_{\text{sim}}(\tilde{\boldsymbol{\theta}})[j]$ for this method.

3.2.1 Simulation of the data-generating system using a finite-difference scheme

In this section, we show how we generate the data points of $\tilde{y}_{\text{sim}}(\tilde{\boldsymbol{\theta}})[j]$ in Equation (9). To this end, we discretise the scaled PDE equations (5) and (6), which will serve two purposes. On the one hand, it provides us a way to generate $\tilde{y}_{\text{sim}}$. On the other hand, the discretisation delivers a state-space model explicit in the physical parameters, which in turn can be converted into a discrete-time

transfer function that is required for optimal experiment design.

PDEs like (5) and (6) are sometimes referred to as *stiff equations*. Applying the wrong integration scheme can result in exponential growth of numerical errors. Most explicit methods, such as the forward Euler method, will only provide a stable solution under restrictive conditions on the spatial and temporal integration steps. To avoid such issues, we have adopted the implicit Crank–Nicolson algorithm, which is known to be unconditionally stable regardless of the temporal and spatial integration steps. A second benefit of this method is that the temporal truncation error is of $(\Delta t)^2$ instead of Δt for the Euler methods.

We recall that we will simulate a scaled version of the data-generating system in Definition 2.1. The conversion between the continuous-time physical models (1)-(2) and (5)-(6) is defined through Equation (4). Using these definitions, the scaled spatial domain becomes $\tilde{\mathcal{D}} = [0, \frac{L}{x_s}]$, which we discretise in M parts of size $\Delta\tilde{x}$. This results in a spatial resolution of $\Delta\tilde{x} = \frac{L}{x_s M}$. The time integration step is chosen equal to $\Delta\tilde{t} = \frac{T_s}{t_s}$[4]. The scaled time is then represented by $\tilde{t} = j\Delta\tilde{t}$, where $j \in \mathbb{N}^+$. We use index $i \in \mathbb{N}^+$ to denote the position on the lattice, i.e. $x_i = i\Delta\tilde{x}$. At location $i\Delta\tilde{x}$ and at time $j\Delta\tilde{t}$, the input and macroscopic field are $\tilde{u}_i^j = \tilde{u}(i\Delta\tilde{x}, j\Delta\tilde{t})$ and $\tilde{f}_i^j = \tilde{f}(i\Delta\tilde{x}, j\Delta\tilde{t})$, respectively. Using these definitions, the scaling steps in Section 2.1, discretisation of Equations (5) and (6) results in

$$\frac{\tilde{f}_i^{j+1} - \tilde{f}_i^j}{\Delta\tilde{t}} = \frac{1}{2}\sum_{l=\{0,1\}}\left(\tilde{\theta}_1\frac{\tilde{f}_{i+1}^{j+l} - 2\tilde{f}_i^{j+l} + \tilde{f}_{i-1}^{j+l}}{(\Delta\tilde{x})^2} + \tilde{\theta}_2\frac{\tilde{f}_{i+1}^{j+l} - \tilde{f}_{i-1}^{j+l}}{\Delta\tilde{x}} + \tilde{\theta}_3\theta_{s,3}t_s\tilde{f}_i^{j+l}\right), \quad (12)$$

$$\tilde{u}_{i_u}^j = -\tilde{\theta}_4\frac{\tilde{f}_{i_u+1}^j - \tilde{f}_{i_u}^j}{\Delta\tilde{x}}, \tilde{y}_{\text{nf}}^j = \tilde{f}_{i_y}^j \quad \text{and } \tilde{f}_{L/x_s}^j = 0\,\forall j, \quad (13)$$

where on the right-hand side (rhs) of the first equation we took the average of a forward and backward Euler methods to ensure stability of the simulation for any $\Delta\tilde{t}$ and $\Delta\tilde{x}$ (it will also ensure stability of the transfer function G that we will derive shortly). Lastly, t_s is defined in step (4) in Section 2.1. This discretisation method is known as the Crank–Nicolson method. We remark that the actuator and sensor positions $\tilde{x}_u$ and $\tilde{x}_y$ in Equation (6) determine the resolution $\Delta\tilde{x}$ to ensure that $i_u = \tilde{x}_u/\Delta\tilde{x}$, $i_y = \tilde{x}_y/\Delta\tilde{x}$ in Equation (13) are integers.

We rewrite the first of the above equations as

$$\begin{aligned}\tilde{f}_i^{j+1} - \tilde{f}_i^j = \tilde{\lambda}_1\left(\tilde{f}_{i+1}^{j+1} - 2\tilde{f}_i^{j+1} + \tilde{f}_{i-1}^{j+1} + \tilde{f}_{i+1}^j - 2\tilde{f}_i^j + \tilde{f}_{i-1}^j\right)\\ + \tilde{\lambda}_2\left(\tilde{f}_{i+1}^{j+1} - \tilde{f}_{i-1}^{j+1} + \tilde{f}_{i+1}^j - \tilde{f}_{i-1}^j\right)\\ + \tilde{\lambda}_3\left(\tilde{f}_i^{j+1} + \tilde{f}_i^j\right), \quad (14)\end{aligned}$$

where the $\tilde{\lambda}$'s are defined as

$$\tilde{\lambda}_1(\tilde{\boldsymbol{\theta}}) = \tilde{\theta}_1\frac{\Delta\tilde{t}}{2(\Delta\tilde{x})^2}, \quad \tilde{\lambda}_2(\tilde{\boldsymbol{\theta}}) = \tilde{\theta}_2\frac{\Delta\tilde{t}}{2\Delta\tilde{x}}, \quad \tilde{\lambda}_3(\tilde{\boldsymbol{\theta}}) = \tilde{\theta}_3\theta_{s,3}t_s\frac{\Delta\tilde{t}}{2}, \quad (15)$$

where we recall that t_s is defined in step (4) in Section 2.1. With these expressions, we will now show how to approximate $\tilde{y}_{\text{nf}}(\tilde{t})$ at discrete-time instances $\tilde{t} = jT_s/t_s$ using the input we applied to the data-generating system $\tilde{u}_{i_u}^j$. To this end, let us denote the vector $\tilde{\boldsymbol{f}}[j+1] = \left(\tilde{f}_0^{j+1}, \ldots, \tilde{f}_M^{j+1}\right)$, which contains the value of the macroscopic field at locations $i = 0, \ldots, M$ at time $j+1$. Similarly, we define $\tilde{\boldsymbol{f}}[j] = \left(\tilde{f}_0^j, \ldots, \tilde{f}_M^j\right)$ for time j. Lastly, we let $\tilde{u}[j+1] = \tilde{u}_{i_u}^{j+1}$ and $\tilde{u}[j] = \tilde{u}_{i_u}^j$. Imposing the boundary conditions (13) and grouping all terms of $j+1$ in Equation (14) on the left-hand side (lhs) and all terms at time j at the rhs results in the *descriptor state-space* form:

$$\tilde{\boldsymbol{\mathcal{E}}}(\tilde{\boldsymbol{\theta}})\tilde{\boldsymbol{f}}[j+1] = \tilde{\boldsymbol{\mathcal{A}}}(\tilde{\boldsymbol{\theta}})\tilde{\boldsymbol{f}}[j] + \tilde{\boldsymbol{\mathcal{B}}}(\tilde{\boldsymbol{\theta}})\left(\tilde{u}[j+1] + \tilde{u}[j]\right), \quad (16)$$

$$\tilde{y}_{\text{sim}}(\tilde{\boldsymbol{\theta}})[j] = \tilde{\boldsymbol{\mathcal{C}}}\tilde{\boldsymbol{f}}[j], \quad (17)$$

in which

$$\tilde{\boldsymbol{\mathcal{E}}}(\tilde{\boldsymbol{\theta}}) = \begin{pmatrix} w_{0,0} & w_1 & 0 & \cdots & \cdots & 0 \\ w_{-1} & w_{0,1} & w_1 & 0 & \cdots & 0 \\ 0 & \ddots & \ddots & \ddots & \ddots & \vdots \\ \vdots & 0 & \ddots & \ddots & \ddots & 0 \\ \vdots & \vdots & \ddots & w_{-1} & w_{0,M-1} & w_1 \\ 0 & 0 & \cdots & 0 & w_{-1} & w_M \end{pmatrix},$$

$$\tilde{\boldsymbol{\mathcal{A}}}(\tilde{\boldsymbol{\theta}}) = \begin{pmatrix} w_{2,0} & -w_1 & 0 & \cdots & \cdots & 0 \\ -w_{-1} & w_{2,1} & -w_1 & 0 & \cdots & 0 \\ 0 & \ddots & \ddots & \ddots & \ddots & \vdots \\ \vdots & 0 & \ddots & \ddots & \ddots & 0 \\ \vdots & \vdots & \ddots & -w_{-1} & w_{2,M-1} & -w_1 \\ 0 & 0 & \cdots & 0 & -w_{-1} & w_{2,M} \end{pmatrix}, \quad (18)$$

$$\tilde{\boldsymbol{\mathcal{B}}}(\tilde{\boldsymbol{\theta}}) = \frac{2\Delta\tilde{x}}{\tilde{\theta}_4}(\tilde{\lambda}_2 - \tilde{\lambda}_1)\left(w_{3,0}, w_{3,1}, \ldots, w_{3,M}\right)^T, \quad \text{and}$$
$$\tilde{\boldsymbol{\mathcal{C}}} = (\delta_{i,i_y}, \delta_{i,i_y}, \ldots, \delta_{i,i_y}). \tag{19}$$

Matrices $\tilde{\boldsymbol{\mathcal{E}}}$ and $\tilde{\boldsymbol{\mathcal{A}}}$ are two $(M+1)\times(M+1)$ matrices, $\tilde{\boldsymbol{\mathcal{B}}}$ a $(M+1)$ column vector and $\tilde{\boldsymbol{\mathcal{C}}}$ a $(M+1)$ row vector. Furthermore,

$$w_{0,i} = 1 + (2 - \delta_{i,i_u})\tilde{\lambda}_1(\tilde{\boldsymbol{\theta}}) - \tilde{\lambda}_3(\tilde{\boldsymbol{\theta}}),$$
$$w_1 = -\tilde{\lambda}_1(\tilde{\boldsymbol{\theta}}) - \tilde{\lambda}_2(\tilde{\boldsymbol{\theta}}), \quad w_{-1} = -\tilde{\lambda}_1(\tilde{\boldsymbol{\theta}}) + \tilde{\lambda}_2(\tilde{\boldsymbol{\theta}}), \tag{20}$$

$$w_{2,i} = 1 - (2 - \delta_{i,i_u})\tilde{\lambda}_1(\tilde{\boldsymbol{\theta}}) + \tilde{\lambda}_3(\tilde{\boldsymbol{\theta}}), \quad w_{3,i} = \delta_{i,i_u}. \tag{21}$$

In the expressions of $w_{0,i}$, $w_{2,i}$ and $w_{3,i}$ the symbol δ_{i,i_u} is the Kronecker delta function, defined by $\delta_{kl} = 1$ if $k = l$ and $\delta^d_{kl} = 0$ for $k \neq l$. It means that the values of $w_{0,i}$, $w_{2,i}$ and $w_{3,i}$ differ at the row index $i = i_u$, which is a consequence of the boundary conditions. We remark that the matrices $\tilde{\boldsymbol{\mathcal{E}}}$ and $\tilde{\boldsymbol{\mathcal{A}}}$ are tri-diagonal since we are dealing with a second-order PDE (cf Equation (1)). Consequently, we can compute the vector $\tilde{\boldsymbol{f}}[j]$ with $O(M)$ complexity with Thomas' algorithm (Thomas, 1949) (a simplified version of Gaussian elimination that can solve tri-diagonal systems of equations).

We now return to the problem of identification in Section 3. To simulate the scaled continuous-time output $\tilde{y}_{\text{nf}}(t)$ defined in Equation (6), we first compute the vector $\tilde{\boldsymbol{f}}[j]$ using Equations (16)–(21) and the scaled input data points from $\tilde{Z}_N$ defined in Section 3, i.e. we compute the macroscopic field $f(x, t)$ at the discrete spatial locations $i\Delta\tilde{x}$ for $i = 0, \ldots, M$, and times $j\Delta\tilde{t} = jT_s/t_s$ for $j = 1, \ldots, N$. Equation (17) then takes the element of this vector corresponding to location $\tilde{x}_y$. Indeed, $\tilde{y}_{\text{sim}}[j]$ is then equivalent to $\tilde{y}_{sim}[j] = \tilde{f}(\tilde{x} = \tilde{x}_y, \tilde{t} = jT_s/t_s)$. We can now identify the physical parameters using Equation (9), the scaled outputs from $\tilde{Z}_N$ and our simulated output $\tilde{y}_{\text{sim}}[j]$. This way of simulating generates the entire macroscopic field $\tilde{f}(x, t)$ at discrete positions $i\Delta\tilde{x}$. The computational time scales linearly with $\Delta\tilde{t}$ due to the tri-diagonal algorithm, which allows for very high spatial resolution in the least-squares identification method.

Lastly, we show how the descriptor state-space form can be converted into a discrete-time transfer function. First, we rewrite system (16)-(17) in its *state-space* form:

$$\tilde{\boldsymbol{f}}[j+1] = \tilde{A}(\tilde{\boldsymbol{\theta}})\tilde{\boldsymbol{f}}[j] + \tilde{B}(\tilde{\boldsymbol{\theta}})\tilde{u}_D[j]$$
$$\tilde{y}_{\text{sim}}(\tilde{\boldsymbol{\theta}})[j] = \tilde{\boldsymbol{C}}\tilde{\boldsymbol{f}}[j], \tag{22}$$

where $\tilde{\boldsymbol{A}}(\tilde{\boldsymbol{\theta}}) = \tilde{\boldsymbol{\mathcal{E}}}^{-1}\tilde{\boldsymbol{\mathcal{A}}}$, $\tilde{\boldsymbol{B}}(\tilde{\boldsymbol{\theta}}) = \tilde{\boldsymbol{\mathcal{E}}}^{-1}\tilde{\boldsymbol{\mathcal{B}}}(1+\tilde{z})$ and $\tilde{\boldsymbol{C}} = \tilde{\boldsymbol{\mathcal{C}}}$. Here, $\tilde{z} = e^{i\tilde{\omega}\tilde{T}_s}$. From this state-space form, we can trivially compute the discrete-time transfer function (the discrete-time equivalent of Equation (7)), being

$$\tilde{G}_{i_u,i_y}(\tilde{z}, \tilde{\boldsymbol{\theta}}) = \tilde{\boldsymbol{C}}[\tilde{z}\boldsymbol{I} - \tilde{\boldsymbol{A}}(\tilde{\boldsymbol{\theta}})]^{-1}\tilde{\boldsymbol{B}}(\tilde{\boldsymbol{\theta}}). \tag{23}$$

In this equation, $\boldsymbol{I}$ is the $(M+1)\times(M+1)$ identity matrix, $\tilde{z} = e^{i\tilde{\omega}\tilde{T}_s}$ and $\tilde{\omega} = \omega t_s$ the scaled frequency. Note that this transfer function is not causal. However, since we only need its frequency response later, and $u(t)$ is fully known, this is not an issue. The discrete-time scaled input and output signals are then related by

$$\tilde{y}_{\text{sim}}(\tilde{\boldsymbol{\theta}})[j] = \tilde{G}_{i_u,i_y}(\tilde{z}, \tilde{\boldsymbol{\theta}})\tilde{u}_D[j]. \tag{24}$$

We recapitulate what we have done so far. We have defined the data-generating system to which we apply an analogue input signal, usually a superposition of sinusoids, and measure the noise-corrupted output at an interval of T_s seconds. We have shown how to identify the physical parameters by scaling the data-set Z_N and simulating the scaled continuous-time model of the data-generating system as defined in Definition 2.1. What we have not yet defined is how to design the input signal that minimises the cost of the experiment while guaranteeing user-imposed constraints on the variances of the physical parameters. This question will be addressed in the next section.

4. Least costly optimal experiment design

We recall that we wish to estimate the true, κ-dimensional, parameter vector $\boldsymbol{\theta}_0$ of the data-generating system (see Definition 2.1) in such a way that the cost of the experiment is minimal, while at the same time guaranteeing with high probability that the variances of the elements of our scaled estimate $\hat{\tilde{\boldsymbol{\theta}}}_N$ remain below certain user-defined constraints. The cost and the constraints need to be a function of the to-be-designed input signal in order to find the optimal one. We first assume that the sensor and actuator locations i_y and i_u are fixed. In all that follows, we consider the scaled system, but conversion to the unscaled system is done with Equation (4). We restrict our attention to a multi-sine input signal.

4.1 Fixed sensor and actuator locations

We start by defining the constraints. The joint confidence region containing an estimate $\hat{\tilde{\boldsymbol{\theta}}}_N$ with a user-defined

probability α is described by the ellipsoid

$$E: \ (\tilde{\boldsymbol{\theta}} - \tilde{\boldsymbol{\theta}}_0)^T P_{\tilde{\boldsymbol{\theta}}}^{-1}[\tilde{\Phi}_{\tilde{u}}](\tilde{\boldsymbol{\theta}} - \tilde{\boldsymbol{\theta}}_0) \leq \chi_\alpha^2(\kappa), \tag{25}$$

in which $\chi_\alpha^2(\kappa)$ is the quantile of the chi-squared distribution function for a probability $\alpha, \kappa = \dim(\tilde{\boldsymbol{\theta}})$. Furthermore, the inverse of the covariance matrix $P_{\tilde{\boldsymbol{\theta}}}^{-1}$ when using the scaled input signal $\tilde{u}_D[n]$ with spectrum $\tilde{\Phi}_{\tilde{u}}$ in the frequency domain reads (Ljung, 1999)

$$\tilde{\boldsymbol{P}}_{\tilde{\boldsymbol{\theta}}}^{-1}[\tilde{\Phi}_{\tilde{u}}(\tilde{\omega})] = \frac{N\tilde{T}_s}{2\pi\tilde{\sigma}_e^2}\int_{-\pi/\tilde{T}_s}^{\pi/\tilde{T}_s}\left[\frac{\partial \tilde{G}_{i_u,i_y}(e^{i\tilde{\omega}\tilde{T}_s},\tilde{\boldsymbol{\theta}})}{\partial\tilde{\boldsymbol{\theta}}}\right]_{\tilde{\boldsymbol{\theta}}=\tilde{\boldsymbol{\theta}}_0} \times \left[\frac{\partial \tilde{G}_{i_u,i_y}(e^{-i\tilde{\omega}\tilde{T}_s},\tilde{\boldsymbol{\theta}})}{\partial\tilde{\boldsymbol{\theta}}}\right]_{\tilde{\boldsymbol{\theta}}=\tilde{\boldsymbol{\theta}}_0}^T \tilde{\Phi}_{\tilde{u}}(\tilde{\omega})\, d\tilde{\omega}, \tag{26}$$

where $\tilde{\sigma}_e^2 = \sigma_e^2/f_s^2$ is the scaled noise variance, $\tilde{G}_{i_u,i_y}(e^{i\tilde{\omega}\tilde{T}_s},\tilde{\boldsymbol{\theta}})$ the discrete-time transfer function defined in Equation (23), $\tilde{T}_s$ the scaled sampling time and $\tilde{\Phi}_{\tilde{u}}(\tilde{\omega})$ the spectrum of input signal.

We now wish to limit the size of this ellipsoid by containing it in a κ-dimensional box defined by the user-defined constraints $\forall i \in [1,\ldots,\kappa]: \ [-\Delta\tilde{\boldsymbol{\theta}}_i + \tilde{\boldsymbol{\theta}}_{0,i}, \Delta\tilde{\boldsymbol{\theta}}_i + \tilde{\boldsymbol{\theta}}_{0,i}]$ to ensure a particular accuracy. These constraints translate into a required variance of the estimates. Let the variance of element i in $\hat{\tilde{\boldsymbol{\theta}}}_{N,i}$ be $\tilde{\sigma}_i^2 = \boldsymbol{e}_i^T\tilde{\boldsymbol{P}}_{\tilde{\boldsymbol{\theta}}}\boldsymbol{e}_i$, where e_i is the ith unit vector, then the constraints can be written as

$$\forall i \in [1,\ldots,\kappa]: \ \tilde{\sigma}_i^2 = \boldsymbol{e}_i^T\tilde{\boldsymbol{P}}_{\tilde{\boldsymbol{\theta}}}\boldsymbol{e}_i \leq \frac{(\Delta\tilde{\theta}_i)^2}{\chi_\alpha^2(\kappa)}. \tag{27}$$

The second component to formulate the least costly experiment design problem is to define the cost of the experiment. We define the scaled cost of the experiment, denoted $\tilde{\mathcal{J}}_{\text{cost}}$, as the power of the as-of-yet undetermined scaled input signal:

$$\tilde{\mathcal{J}}_{\text{cost}}[\tilde{\Phi}_{\tilde{u}}] = \frac{\tilde{T}_s}{2\pi}\int_{-\pi/\tilde{T}_s}^{\pi/\tilde{T}_s}\tilde{\Phi}_{\tilde{u}}(\tilde{\omega})\, d\tilde{\omega}. \tag{28}$$

The least costly experiment design problem is thus formulated as

$$\min_{\tilde{\Phi}_{\tilde{u}}} \tilde{\mathcal{J}}_{\text{cost}}[\tilde{\Phi}_{\tilde{u}}] \tag{29}$$

subject to the constraints (27):

$$\forall i: \ \begin{pmatrix} \dfrac{(\Delta\tilde{\theta}_i)^2}{\chi_\alpha^2(\kappa)} & \boldsymbol{e}_i^T \\ \boldsymbol{e}_i & \tilde{\boldsymbol{P}}_{\tilde{\theta}}^{-1}[\tilde{\Phi}_{\tilde{u}}] \end{pmatrix} \succeq 0. \tag{30}$$

Observe that we have rewritten constraint (27) into (30) by invoking Schur's complement in order to ensure that all constraints are linear in the spectrum $\tilde{\Phi}_{\tilde{u}}$, i.e. we have linear matrix inequalities (LMIs). Consequently, since the cost is also linear in the spectrum, the optimisation problem (29)-(30) is linear in the design variable $\tilde{\Phi}_{\tilde{u}}$. The optimisation problem is thus convex. Its solution, denoted $\tilde{\Phi}_{\tilde{u},\text{opt}}$, is the spectrum that minimises the cost while honouring the constraints. In order to solve this problem numerically, we have to parameterise the input spectrum $\tilde{\Phi}_{\tilde{u}}(\tilde{\omega})$. To this end, we discretise the frequency domain into $Q \in \mathbb{N}^+$ parts. Defining $\tilde{\omega}_f = \frac{\pi}{Q\tilde{T}_s}$ as the fundamental frequency, we have that $\tilde{\omega}_l = l\tilde{\omega}_f$, for $l = 1,\ldots,Q_{\text{ex}}$, where $Q_{\text{ex}} \leq Q$ is the number of sinusoids used in experiment design.[5] Furthermore, we choose the spectrum to be of the following form:

$$\tilde{\Phi}_{\tilde{u}}(\tilde{\omega}) = \frac{\pi}{2\tilde{T}_s}\sum_{l=1}^{Q_{\text{ex}}}\tilde{A}_l^2\left[\delta(\tilde{\omega} - l\tilde{\omega}_f) + \delta(\tilde{\omega} + l\tilde{\omega}_f)\right], \tag{31}$$

corresponding to a $Q\tilde{T}_s/2$-periodic discrete-time multi-sine

$$\tilde{u}[j] = \tilde{u}(j\tilde{T}_s) = \sum_{l=1}^{Q_{\text{ex}}}\tilde{A}_l\sin(l\tilde{\omega}_f j\tilde{T}_s). \tag{32}$$

Substitution of Equation (31) into the cost (29) and the expression of the covariance matrix (26) gives

$$\tilde{\mathcal{J}}_{\text{cost}}[\tilde{\Phi}_{\tilde{u}}] = \frac{1}{2}\sum_{l=1}^{Q_{\text{ex}}}\tilde{A}_l^2 \tag{33}$$

and

$$\tilde{\boldsymbol{P}}_{\tilde{\boldsymbol{\theta}}}^{-1} = \frac{N}{2\tilde{\sigma}_e^2}\sum_{l=1}^{Q_{\text{ex}}}\tilde{A}_l^2\text{Re}\left\{\left[\frac{\partial \tilde{G}_{i_u,i_y}(e^{il\tilde{\omega}_f\tilde{T}_s},\tilde{\boldsymbol{\theta}})}{\partial\tilde{\boldsymbol{\theta}}}\right]_{\tilde{\boldsymbol{\theta}}=\tilde{\boldsymbol{\theta}}_0} \times \left[\frac{\partial \tilde{G}_{i_u,i_y}(e^{-il\tilde{\omega}_f\tilde{T}_s},\tilde{\boldsymbol{\theta}})}{\partial\tilde{\boldsymbol{\theta}}}\right]_{\tilde{\boldsymbol{\theta}}=\tilde{\boldsymbol{\theta}}_0}^T\right\}. \tag{34}$$

The above two equations show that the cost and covariance matrix are now linear in the amplitudes $\tilde{A}_l^2$. Substitution into the optimisation problems (29) and (30) then yields a convex finite-dimensional problem in $\tilde{A}_l^2$. The integer Q determines the accuracy of the solution. In Appendix 3, we show how to compute the gradient $\partial\tilde{G}_{i_u,i_y}/\partial\tilde{\boldsymbol{\theta}}$ efficiently. The solution to the optimisation problem generates the set $\{\tilde{A}_{l,\text{opt}}\}_{l=1,\ldots,Q_{\text{ex}}}$. Substitution of these amplitudes in Equation (32) then delivers the scaled optimal input signal $\tilde{u}_{\text{opt}}[j]$. The unscaled optimal input signal is easily retrieved via Equation (4), i.e.

$A_{l,\text{opt}} = \tilde{A}_{l,\text{opt}} u_s$ and $\omega_l = \tilde{\omega}_l / t_s$. The resulting unscaled signal is the analogue equivalent of Equation (32).

We finish this part with some remarks.

First, observe that the constraint (27) and the inverse of the covariance matrix (26) depend on the unknown true parameter values $\tilde{\boldsymbol{\theta}}_0$. Stated otherwise: to design the optimal input signal that identifies the parameters we already need to know them. This so-called chicken-and-egg problem is in practice circumvented by replacing $\tilde{\boldsymbol{\theta}}_0$ in these equations by an initial guess, $\tilde{\boldsymbol{\theta}}_g$. Admittedly, this will by definition result in different experiment costs and different parameter variances. Nevertheless, under equal input power, the framework can deliver signals that result in variances of the parameters that are lower than obtained with an arbitrary input signal. An illustration will follow in Section 5.

Second, we mentioned in the introduction that scaling is of importance in the least costly experiment design framework for physical systems. We comment further on this now. Suppose we want to identify two physical parameters, denoted θ_1 and θ_2. Their values can easily differ by 10 orders of magnitude, resulting in variances (that are on the diagonal of $\boldsymbol{P}_\theta$) that differ by 20 orders of magnitude. Consequently, the matrix $\boldsymbol{P}_\theta^{-1}$ is ill-posed, and the convex methods can no longer solve such problems. However, with scaling, the parameters are of the same order, resolving the badly scaled matrix.

Third, the LMI optimisation problem can be solved in polynomial time. The number of decision variables Q_{ex} is not big, as well as the number of to-be-identified parameters. This leads to rather quick solutions.

Lastly, we mention that in the numerical procedure we require an expression for $\partial \tilde{G}_{i_u,i_y}(\tilde{z}, \tilde{\boldsymbol{\theta}}_0)/\partial \tilde{\boldsymbol{\theta}}$. The transfer function $\tilde{G}_{i_u,i_y}(\tilde{z}, \tilde{\boldsymbol{\theta}}_0)$ being of high order for fine spatial grids, this can lead to a heavy computational load. Note that nevertheless, as previously mentioned, this load can be eased by the method described in Appendix 3. Moreover, it is also to be noted that this gradient computation can be achieved prior to the resolution of the LMI problem. Finally, this load becomes negligible if an explicit continuous-time expression for $\tilde{G}_{i_u,i_y}(i\tilde{\omega}, \tilde{\boldsymbol{\theta}}_0)$ exists. Indeed, the discrete-time transfer function in Equation (26) can then be replaced by its much simpler continuous-time equivalent. We give an example in Section 5.

4.2 Actuator and sensor locations as design variables

In the previous section, we formulated the least-costly experiment design (LCED) framework but assumed that the actuator and sensor locations i_u and i_y were given. Since the derivatives of $\tilde{G}_{i_u,i_y}$ (23) depend explicitly on the actuator and sensor locations, we can also attempt to decrease the cost even further by optimally choosing these locations. Due to the explicit dependence of the derivatives on the locations, the optimal frequencies change with the locations. Consequently, we have to solve the LCED optimisation problem formulated in the previous section for many combinations of i_u and i_y.

Set N_{sim} as total number of iterations;
Set α and $\Delta\theta_i$'s to set constraints;
Set Q determining the lowest frequency $\omega_f = \frac{\pi}{QT_s}$;
Set array $\tilde{\mathbf{A}}_{\text{opt}} = [\tilde{A}_l]_{l=1,\ldots,Q_{\text{ex}}}$;
Set array $\tilde{\mathbf{x}}_{\text{opt}} = [\tilde{x}_u, \tilde{x}_y]$;
Set cost $\tilde{\mathcal{J}}_{\text{opt}} = 1 \times 10^8$ (a high value);
$\tilde{x}_{u,\text{sub}} = \frac{1}{2}$, $\tilde{x}_{y,\text{sub}} = \frac{1}{2}$;
$k = 0$;
while $k < N_{\text{sim}}$ **do**
  $\Delta x_{u,k} = \tilde{x}_{u,\text{sub}}$, $\Delta x_{y,k} = \tilde{x}_{y,\text{sub}}$;
  for $i = 1$ *to* 2 **do**
    $x_u = (i-1)\Delta x_{u,k} + \frac{1}{2}\Delta x_{u,k}$;
    for $j = 1$ *to* 2 **do**
      $x_y = (j-1)\Delta x_{y,k} + \frac{1}{2}\Delta x_{y,k}$;
      Solve Equations (29) and (30) using Equation (31) and use solution $\tilde{\boldsymbol{A}} = \left\{\tilde{A}_l\right\}_{l=1,\ldots,Q_{\text{ex}}}$ to compute cost $\tilde{\mathcal{J}}_{\text{cost}}[\tilde{\boldsymbol{A}}]$ (28);
      if $\tilde{\mathcal{J}}_{\text{cost}}[\tilde{\boldsymbol{A}}] < \tilde{\mathcal{J}}_{\text{opt}}$ **then**
        $\tilde{x}_{u,\text{sub}} = x_u$, $\tilde{x}_{y,\text{sub}} = x_y$;
        $\tilde{\mathbf{A}}_{\text{opt}} = \tilde{\mathbf{A}}$;
        $\tilde{\mathcal{J}}_{\text{opt}} = \tilde{\mathcal{J}}_{\text{cost}}$;
      end
    end
  end
  $\boldsymbol{x}_{\text{opt}} = [x_{u,\text{sub}}, x_{y,\text{sub}}]$;
  $k = k + 1$;
end

Algorithm 1: Progressive subdivision algorithm that finds the minimal experiment cost by designing the optimal input spectrum and optimal sensor and actuator locations.

The solution of this algorithm is given by the set of values $\{\tilde{\boldsymbol{x}}_{\text{opt}}, \tilde{\boldsymbol{A}}_{\text{opt}}, \tilde{\mathcal{J}}_{\text{opt}}\}$ containing the optimal actuator and sensor location, as well as the optimal amplitudes and the optimal cost. Conversion to the unscaled signal is described in the previous section.

The algorithm makes use of progressive subdivision. The algorithm starts by dividing the (x_u, x_y)-plane into

four equally sized squares. For each square, the optimisation problem is solved at the coordinates that correspond to the centre of the square. From these four solutions the one that delivers the smallest cost $\mathcal{J}_{\text{cost}}$ is selected. At step $k+1$, that square is subsequently divided into four equally sized squares for which we again find the least costly solution. This procedure is repeated until N_{sim} divisions have taken place. This subdivision algorithm is important if the number of variables such as $\tilde{x}_u$ and $\tilde{x}_y$ increases. The algorithm is easily adapted if only one spatial degree is considered (only input or output location).

The algorithm speed can be improved drastically in cases where $\dim(\boldsymbol{\theta}) \leq 2$, for which we derived analytical solutions in Potters, Forgione, Bombois, and van den Hof (2015) and a novel analytical solution in Appendix 2. A properly chosen frequency grid can further improve the speed.

4.2.1 Example: estimating the dispersion coefficient and reaction rate in a tracer experiment

As the first numerical illustration of our result, let us consider a 1D river containing a homogeneous fluid (Didierjean, Maillet, & Moyne, 2004). For the sake of brevity, we will directly consider the scaled system. The river is modelled as an infinite medium with a constant flow speed $\tilde{v}_0 = 3$. Following Didierjean et al. (2004), we consider the following experiment: we inject a tracer with a rate $\tilde{q}(\tilde{x}, \tilde{t})$ in the river (on, for example, a boat) at a stationary position $\tilde{x} = \tilde{x}_u$ and measure the tracer concentration $\tilde{c}(\tilde{x}, \tilde{t})$ (with, for example, another boat) downstream at position $\tilde{x} = \tilde{x}_y \geq \tilde{x}_u$. The input $\tilde{u}(\tilde{t}) = \tilde{q}(\tilde{x}_u, \tilde{t})$ and the output $\tilde{y}(\tilde{t}) = \tilde{c}(\tilde{x}_y, \tilde{t})$.

The dynamics are governed by Equation (5) where the profile $\tilde{f}(\tilde{x}, \tilde{t})$ is here the concentration $\tilde{c}(\tilde{x}, \tilde{t})$, and parameter $\tilde{\theta}_1$ is the so-called dispersion coefficient $\tilde{\eta}$, $\tilde{\theta}_2$ the flow speed $\tilde{v}$ and $\tilde{\theta}_3$ the reaction rate $\tilde{\xi}$. The boundary conditions involves the tracer injection rate $\tilde{q}(\tilde{x}_u, \tilde{t})$ and are a bit different than in Equation (6) (see Didierjean et al., 2004). Among the three parameters, the flow speed $\tilde{v}$ is generally not identified from data, but measured. Consequently, our aim will be to identify the two remaining parameters: the dispersion coefficient and the reaction rate of the tracer. Note that the dispersion coefficient represents the combined effect of molecular diffusion and hydrodynamic transport.

As shown in Didierjean et al. (2004), one can deduce a closed form of the continuous-time transfer function between the input and output. After scaling, we obtain

$$\tilde{G}_{\tilde{l}}(\tilde{s}, \tilde{\boldsymbol{\theta}}) = \left[\frac{A(\tilde{s}, \tilde{\boldsymbol{\theta}})}{Z_{-\infty}(\tilde{\boldsymbol{\theta}})} + \frac{B(\tilde{s}, \tilde{\boldsymbol{\theta}})}{Z_{-\infty}(\tilde{\boldsymbol{\theta}}) Z_{+\infty}(\tilde{\boldsymbol{\theta}})} + C(\tilde{s}, \tilde{\boldsymbol{\theta}}) + \frac{D(\tilde{s}, \tilde{\boldsymbol{\theta}})}{Z_{+\infty}(\tilde{\boldsymbol{\theta}})} \right]^{-1} \exp\left(\frac{\tilde{v}\tilde{l}}{2\tilde{\eta}} \right), \tag{35}$$

where $\tilde{l} = \tilde{x}_y - \tilde{x}_u$ is the distance between the measurement and actuator location, and

$$\begin{aligned} A(\tilde{s}, \tilde{\boldsymbol{\theta}}) &= \left[\cosh\left(\tilde{k}\tilde{l}\right) - \frac{\tilde{v}}{2\tilde{k}\tilde{\eta}} \sinh\left(\tilde{k}\tilde{l}\right) \right], \\ B(\tilde{s}, \tilde{\boldsymbol{\theta}}) &= \frac{1}{\tilde{k}\tilde{\eta}} \sinh\left(\tilde{k}\tilde{l}\right), \\ C(\tilde{s}, \tilde{\boldsymbol{\theta}}) &= \frac{\tilde{s}}{\tilde{k}} \sinh\left(\tilde{k}\tilde{l}\right), \quad D(\tilde{s}, \tilde{\boldsymbol{\theta}}) \\ &= \left[\cosh\left(\tilde{k}\tilde{l}\right) + \frac{\tilde{v}}{2\tilde{k}\tilde{\eta}} \sinh\left(\tilde{k}\tilde{l}\right) \right], \end{aligned} \tag{36, 37}$$

$$Z_{\pm\infty} = \frac{1}{\tilde{k}\tilde{\eta} - \tilde{v}/2}, \quad \tilde{k}(\tilde{s}, \tilde{\boldsymbol{\theta}}) = \sqrt{\frac{\tilde{s} - \tilde{\xi}}{\tilde{\eta}} + \frac{\tilde{v}^2}{4\tilde{\eta}^2}}. \tag{38}$$

Observe that the transfer function is only a function of the relative distance of the actuator to the sensor. This makes sense, as it should not matter where we inject the tracer in an infinitely long river.

Let us define the data-generating system with the parameter vector $\tilde{\boldsymbol{\theta}} = [\tilde{\eta}_0, \tilde{\xi}_0] = [1.0, -0.1]$ and assume that $\tilde{v}_0 = 3$. Our objective is to estimate $\tilde{\boldsymbol{\theta}}_0$. The scaled measurement noise is assumed to be $\tilde{\sigma}_e^2 = 0.01$; the experiment length is set to $N = 9000$ samples. We wish to identify $\tilde{\boldsymbol{\theta}}$ with the least powerful input signal, yet ensuring that the parameter variance constraints $\tilde{\sigma}_{\tilde{\eta}}^2 \leq \left(\frac{0.01}{3}\right)^2$ and $\tilde{\sigma}_{\tilde{\xi}}^2 \leq \left(\frac{0.02}{3}\right)^2$ are satisfied. To this end, we also optimise the distance $\tilde{l}$ between the actuator and the sensor.

The distance $\tilde{l}$ is a scalar variable, hence Algorithm 1 need not be used to determine the optimal distance. We instead solve the optimisation problems (28)–(30) for the values $\tilde{l} = 0, 0.05, 0.1, \ldots, 1.5$. Since only two parameters are identified, we can use the analytical solution in Appendix 2 to solve the problem for all these values of $\tilde{l}$. However, we could of course also have used the LMI optimisation.

Using this procedure, the least powerful excitation signal is found for a distance $\tilde{l}_{\text{opt}} = 1.0$. For this value, the least powerful excitation signal is given by

$$\tilde{u}(\tilde{t}) = \tilde{A}_{\text{opt}} \sin(\tilde{\omega}_{\text{opt}} \tilde{t}), \tag{39}$$

where $\tilde{A}_{\text{opt}} = 7.54$, $\tilde{\omega}_{\text{opt}} = 0.31$.

The optimal (scaled) amplitude is thus equal to 7.34 for $\tilde{l}_{\text{opt}}$. For $\tilde{l} = 0$, the amplitude that is required to fulfil the variance constraints is 15.16, i.e. twice as much. For distances exceeding $\tilde{l}_{\text{opt}}$, the amplitude also increases significantly. This shows the advantage of optimising the distance between the sensor and actuator in this experiment.

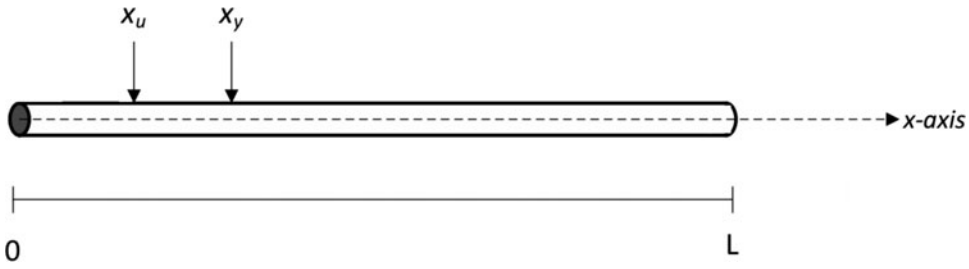

Figure 2. Sketch of the experimental set-up. The actuator location is indicated with x_u, the sensor location with x_y. The left end of the rod with length L is put at $x = 0$.

In the next section, we consider a more detailed example and compare our results with existing ones in the literature.

5. Case study: estimation of diffusivity and conductivity parameters in front-face experiments

In this section, we apply the optimal experiment design framework to the identification of thermal parameters with a front-face experiment. The experimental set-up is inspired by work of Gabano and Poinot (2009) and simulated with the computer. We first introduce the data-generating system and its scaled equivalent in Section 5.1. We then set up the experiment and define the constraints on the variances of the estimates and compute the optimal input signal in Section 5.2. We solve the optimisation problem using CVX (Grant & Boyd, 2013). We also show what the optimal actuator and sensor locations are. In Section 5.3, the optimal input signal is applied to the data-generating system (in a simulation environment) and with the collected data we identify the physical parameters. In order to test if the variance constraints are honoured, we simulate 2×10^4 experiments. We also analyse what happens to the optimal input signal when we replace $\tilde{\boldsymbol{\theta}}_0$ by an initial guess $\tilde{\boldsymbol{\theta}}_g$ in Equation (34).

5.1 Data-generating system

We consider a homogeneous rod of length $L = 0.05$m oriented along the spatial coordinate x (see Figure 2). We place the left side of the rod at $x = 0$, such that the spatial domain we consider is $\mathcal{D} = [0, L]$. During the experiment, we heat the cross-sectional area of the rod uniformly at $x = x_u$ with a heat flux $u(t)$ and keep the temperature constant at the right boundary ($x = L$), here equal to zero.[6] We measure the temperature $T(x, t)$ at position $x = x_y \in \mathcal{D}$. The optimal actuator and sensor positions are determined with optimal experiment design. We assume zero initial conditions.

The dynamics are governed by the following equations:

$$\frac{\partial T(x,t)}{\partial t} = \alpha_0 \frac{\partial^2 T(x,t)}{\partial x^2}, \tag{40}$$

$$-\lambda_0 \left.\frac{\partial T(x,t)}{\partial x}\right|_{x=x_u} = u(t),\ y_{\mathrm{nf}}(t) = T(x_y,t),\ \text{and}$$

$$T(L,t) = 0\,\forall t, \tag{41}$$

in which $\lambda_0 = 111\ \mathrm{Wm^{-1}{}^{\circ}C^{-1}}$ is the thermal conductivity and $\alpha_0 = 3.38 \times 10^{-5}\ \mathrm{m^2 s^{-1}}$ the thermal diffusivity. We collect the physical parameters in the vector $\boldsymbol{\theta}_0 = [\alpha_0, \lambda_0]$. This data-generating system corresponds to the continuous-time second-order PDEs (1) and (2) for the macroscopic field $f(x, t) = T(x, t)$, input location $x = x_u$, $\theta_{1,0} = \alpha_0$ and $\theta_{4,0} = \lambda_0$. Our goal is to identify the physical parameters $\boldsymbol{\theta}_0 = [\alpha_0, \lambda_0] = [3.38 \times 10^{-5}, 111]$.

5.1.1 Non-dimensionalisation

Following Section 2.1, we introduce the non-dimensional variables $\tilde{T}(\tilde{x}, \tilde{t}) = \frac{T(x,t)}{y_s}, \tilde{x} = \frac{x}{x_s}, \tilde{u}(\tilde{t}) = \frac{u(t)}{u_s}, \tilde{t} = \frac{t}{t_s}$, and non-dimensional parameters $\tilde{\alpha}_0 = \frac{\alpha_0}{\alpha_s}$, $\tilde{\lambda}_0 = \frac{\lambda_0}{\lambda_s}$. Choosing $y_s = 1$, $x_s = L = 0.05$, $t_s = \frac{L^2}{\alpha_0} = 73.96$, $u_s = \frac{L}{\lambda_0 y_s} = 4.5 \times 10^{-4}$, $\alpha_s = \alpha_0$, $\lambda_s = \lambda_0$, and substituting the non-dimensional variables in Equations (40) and (41) results in the non-dimensional model,

$$\frac{\partial \tilde{T}(\tilde{x},\tilde{t})}{\partial \tilde{t}} = \tilde{\alpha}_0 \frac{\partial^2 \tilde{T}(\tilde{x},\tilde{t})}{\partial \tilde{x}^2}, \tag{42}$$

$$-\tilde{\lambda}_0 \left.\frac{\tilde{T}(\tilde{x},\tilde{t})}{\partial \tilde{x}}\right|_{\tilde{x}=\tilde{x}_u} = \tilde{u}(\tilde{t}),\ \tilde{y}_{\mathrm{nf}}(\tilde{t}) = \tilde{T}(\tilde{x}_y,\tilde{t}),\ \text{and}$$

$$\tilde{T}(1,\tilde{t}) = 0\,\forall \tilde{t}. \tag{43}$$

Note that we have used an initial guess $\boldsymbol{\theta}_g = \boldsymbol{\theta}_0$ for convenience. This results in an unscaled true parameter vector, $\tilde{\boldsymbol{\theta}}_0$, that is of $O(1)$.

The non-dimensional continuous-time transfer function $\tilde{G}_{\tilde{x}_u,\tilde{x}_y}(\tilde{s}, \tilde{\boldsymbol{\theta}}_0)$ that couples $\tilde{u}(\tilde{t})$ to the output $\tilde{y}_{\mathrm{nf}}(\tilde{t})$ (cf

Equation (7)) is derived in Appendix 1 and reads as

$$\tilde{G}_{\tilde{x}_u,\tilde{x}_y}(\tilde{s},\tilde{\boldsymbol{\theta}}_0) = \frac{1}{\tilde{\lambda}_0}\sqrt{\frac{\tilde{\alpha}_0}{\tilde{s}}}\frac{\sinh\left(\sqrt{\frac{\tilde{s}}{\tilde{\alpha}_0}}(1-\tilde{x}_y)\right)}{\cosh\left(\sqrt{\frac{\tilde{s}}{\tilde{\alpha}_0}}(1-\tilde{x}_u)\right)}. \tag{44}$$

In this equation, the Laplace variable has also been scaled according to Equation (4), i.e. $\tilde{s} = t_s s = sL^2/\alpha_0$. We will use this transfer function in the experiment design procedure that is explained in the next section.

5.2 Experiment preliminaries

In this section, we define the experiment. We choose the same parameters as in Gabano and Poinot (2009), mainly to compare the excitation frequencies. We remark that we did not have an actual physical set-up to generate data. Instead, the noise-corrupted output data is generated with the computer. We set the experiment length at $N = 2000 + 9000$ samples, where the first 2000 samples are not used in the identification, i.e. we wait until transients died out. The sampling time is set at $T_s = 0.1$ s. The optimal input signal (which we will compute shortly) generates the measured output of the data-generating system given by

$$y_D[n] = y_{\text{nf}}(nT_s) + e(nT_s), \tag{45}$$

where we assumed that the output of the data-generating system $y_{\text{nf}}(nT_s)$ is corrupted by zero-mean Gaussian white noise with variance $\sigma_e^2 = 0.05$ (see also Equation (8)).

5.2.1 Optimal experiment design

In Gabano and Poinot (2009), the collection of a thousand estimates $\{\hat{\alpha}_N\}$ and $\{\hat{\lambda}_N\}$ were distributed around their respective true values $\alpha_0 = 3.38 \times 10^{-5}$ and $\lambda_0 = 111$ (identical to the parameters used in this section) with $\sigma_\alpha = 0.02\alpha_0/3$ and $\sigma_\lambda = 0.01\lambda_0/3$. Following Section 4, we cast these values in the scaled variance constraints (27):

$$\tilde{\sigma}_{\tilde{\alpha}}^2 \equiv \tilde{\sigma}_1^2 \le \left(\frac{0.02}{3}\right)^2, \tilde{\sigma}_{\tilde{\lambda}}^2 \equiv \tilde{\sigma}_2^2 \le \left(\frac{0.01}{3}\right)^2, \tag{46}$$

where it is understood that the probability $\alpha \approx 0.99$, and that $\chi^2_{0.99}(2) \approx 9$. The optimal experiment design problem is formulated by Equations (29) and (30). Choosing Equation (31) to represent the scaled spectrum, the above constraints, the scaled optimisation problem for this experiment reads

$$\min_{\{\tilde{A}_l\}} \frac{1}{2}\sum_{l=1}^{Q_{\text{ex}}} \tilde{A}_l^2 \tag{47}$$

subject to the constraints

$$\begin{pmatrix} \tilde{\sigma}_\alpha^2 & \boldsymbol{e}_1^T \\ \boldsymbol{e}_1 & \tilde{\boldsymbol{P}}_{\tilde{\boldsymbol{\theta}}}^{-1} \end{pmatrix} \succeq 0, \begin{pmatrix} \tilde{\sigma}_\lambda^2 & \boldsymbol{e}_2^T \\ \boldsymbol{e}_2 & \tilde{\boldsymbol{P}}_{\tilde{\boldsymbol{\theta}}}^{-1} \end{pmatrix} \succeq 0. \tag{48}$$

The expression of $\tilde{\boldsymbol{P}}_{\tilde{\boldsymbol{\theta}}}^{-1}$ is given by Equation (34), in which we substituted $\tilde{G}_{i_u,i_y}(\tilde{z},\tilde{\boldsymbol{\theta}})$ with the continuous-time transfer function $\tilde{G}_{\tilde{x}_u,\tilde{x}_y}(\tilde{s},\tilde{\boldsymbol{\theta}})$ in Equation (44), and used as initial guess $\boldsymbol{\theta}_g = \boldsymbol{\theta}_0$, i.e. $\tilde{\boldsymbol{\theta}}_0 = [1.0, 1.0]$.

We use Algorithm 1 to find the optimal locations and the optimal input signal for those locations. To this end, we thus solve the problem (29)-(30) with the LMI approach. We take $Q = Q_{\text{ex}} = 200$. For each combination $(\tilde{x}_u, \tilde{x}_y)$, it turns out that the optimal input signal is a single sinusoid. Interestingly, we find that the lowest cost, i.e. $\tilde{\mathcal{J}}_{\text{cost}} = \frac{1}{2}\tilde{A}_{\text{opt}}^2$ is obtained at $(\tilde{x}_u, \tilde{x}_y) = (0, 0.12)$. The optimal amplitude $\tilde{A}_{\text{opt}}$ at $\tilde{x}_u = 0$ as a function of $\tilde{x}_y$) is depicted in Figure 3(a). In unscaled length, this corresponds to $x_y = 0.12L$. In practice, front-face experiments ($x_u = x_y = 0$) are common. However, this study suggests that this is not the best practice, as a lower cost (proportional to $\tilde{A}^2$) of about 6% can be obtained at $\tilde{x}_y = 0.12$. Equivalently, for the same cost, the variances in the parameters will be about 6% lower since $\tilde{P}_{\tilde{\boldsymbol{\theta}}}^{-1}$ is proportional to $\tilde{A}^2$. Furthermore, observe that the curve increases rapidly as $\tilde{x}_y$ increases. Although not shown in the figure, when $\tilde{x}_y \to 1$, the optimal amplitude $\tilde{A}_{\text{opt}} \to \infty$. This is a consequence of the boundary condition $\tilde{T}(1,\tilde{t}) = 0\,\forall\tilde{t}$ (cf Equation (43)). Hence, the informativeness of the data at any frequency is zero at this location.

Although the best estimate can be obtained at $(\tilde{x}_u, \tilde{x}_y) = (0, 0.12)$, we shall, however, use the optimal input signal for $\tilde{x}_u = 0$ and sensor location $\tilde{x}_y = 0$ to compare with previous works. In this case, the optimal input signal is computed to be

$$\tilde{u}_{\text{opt}}(\tilde{t}) = 1.7067\sin(1.5666\tilde{t}), \tag{49}$$

which in unscaled variables translates (using the conversion defined in Section 5.1) into the optimal input signal[7]

$$\tilde{u}_D(\tilde{t}) = 3.789 \times 10^3 \sin(0.0212t). \tag{50}$$

Observe from Figure 3(b) that the scaled optimal frequency $\tilde{\omega} = 1.5666$ lies in between the two maxima of the

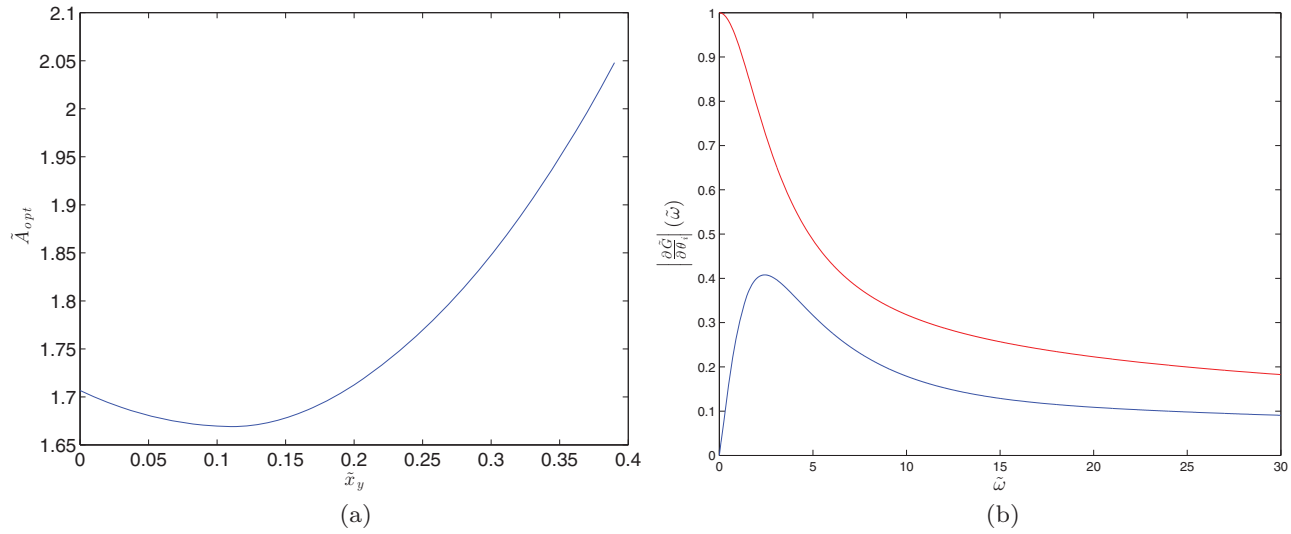

Figure 3. (a) The optimal input signal is a single sinusoid of which the logarithm of the optimal amplitude $\tilde{A}_{\text{opt}}$ is plotted against the sensor position $\tilde{x}_y$ for $\tilde{x}_u = 0$. (b) Derivatives $\partial \tilde{G}_{\tilde{x}_u,\tilde{x}_y}(i\tilde{\omega}, \tilde{\boldsymbol{\theta}})/\partial\tilde{\alpha}$ (red) and $\partial \tilde{G}_{\tilde{x}_u,\tilde{x}_y}(i\tilde{\omega}, \tilde{\boldsymbol{\theta}})/\partial\tilde{\lambda}$ (blue) for $\tilde{x}_u = \tilde{x}_y = 0$.

derivatives of $\tilde{G}_{\tilde{x}_u,\tilde{x}_y}$. This is an intuitively pleasing result, as high values for the derivatives lead to a large certainty (see Equation (34)). We refer the reader to Appendix 2 for a more detailed analysis and interpretation of the optimal input signal.

5.2.2 Chicken-and-egg problem

The optimal input signal designed in the previous section was designed by using the true parameter vector $\tilde{\boldsymbol{\theta}}_0$. In practice, however, we obviously do not know this vector as we in fact want to estimate it. As mentioned in Section 4, the problem of finding the optimal signal to identify the parameter vector requires the parameter vector itself. This so-called chicken-and-egg problem can be circumvented by replacing $\tilde{\boldsymbol{\theta}}_0$ in Equation (34) with a previous estimate or guess $\tilde{\boldsymbol{\theta}}_g$. This inevitably leads to a designed input signal that is not optimal. Optimal input design can, however, still be used and will generally lead to better estimates than arbitrary signals under the same experiment cost.

A central question is the sensitivity of the cost of the experiment to the initial guess $\tilde{\boldsymbol{\theta}}_g$, and whether or not the constraints will still be honoured. To this end we computed the optimal amplitude and frequency for many values of $\tilde{\boldsymbol{\theta}}_g$ using Equations (47) and (48). The range in which these values lie is larger than the desired accuracy of estimates from the identification experiment. In Figure 4(a), the optimal amplitude is shown for values of $\tilde{\lambda}$ and $\tilde{\alpha}$ around 10% of $\tilde{\lambda}_0 = 1$ and $\tilde{\alpha}_0 = 1$ (the case for which $\boldsymbol{\theta}_g = \boldsymbol{\theta}_0$). Observe that within this range the optimal amplitudes can differ up to 30% from the one obtained with $\tilde{\boldsymbol{\theta}}_0 = \tilde{\boldsymbol{\theta}}_g$, i.e. $A_{\text{opt}} = 1.7067$ (cf Equation (49)). The cost of the experiment is thus rather sensitive to the guess $\tilde{\boldsymbol{\theta}}_g$. In Figure 4(b), the optimal frequencies as a function of $\tilde{\boldsymbol{\theta}}_g$ are shown. It can be observed that the optimal frequency is not sensitive to a wrong guess $\tilde{\alpha}_g$ for a given guess $\tilde{\lambda}_g$.

To test whether the constraints will still be honoured, and how large the error in the estimates is when using the optimal input signal designed with $\boldsymbol{\theta}_g \neq \boldsymbol{\theta}_0$, we proceed as follows. For each guess $\tilde{\boldsymbol{\theta}}_g$, we use the corresponding optimal amplitude and frequency of Figure 4(a) and 4(b) and apply this input signal to the true system. We then obtain the variances in the estimates $\hat{\tilde{\alpha}}_N$ and $\hat{\tilde{\lambda}}_N$ as a function of $\tilde{\boldsymbol{\theta}}_g$. We use the following measure of error:

$$e(\tilde{\boldsymbol{\theta}}_g) = \frac{1}{2}\left[\frac{\text{var}\hat{\tilde{\alpha}}_N(\tilde{\alpha}_g) - \text{var}\hat{\tilde{\alpha}}_N(\tilde{\alpha}_0)}{\text{var}\hat{\tilde{\alpha}}_N(\tilde{\alpha}_0)} + \frac{\text{var}\hat{\tilde{\lambda}}_N(\tilde{\lambda}_g) - \text{var}\hat{\tilde{\lambda}}_N(\tilde{\lambda}_0)}{\text{var}\hat{\tilde{\lambda}}_N(\tilde{\lambda}_0)}\right]. \tag{51}$$

We found that the relative error in the considered interval lies between 0% and 30%. Also, it is clear that a strong correlation exists with Figure 4(a): if the optimal amplitude is larger or equal to $\tilde{A}_{\text{opt}} = 1.7067$ ($(\tilde{\alpha}, \tilde{\lambda}) = (1, 1)$), we obtain variances that are smaller or equal to the case $\boldsymbol{\theta}_g = \boldsymbol{\theta}_0$. Conversely, we do not satisfy the constraints if the optimal amplitude is smaller than $\tilde{A}_{\text{opt}} = 1.7067$.

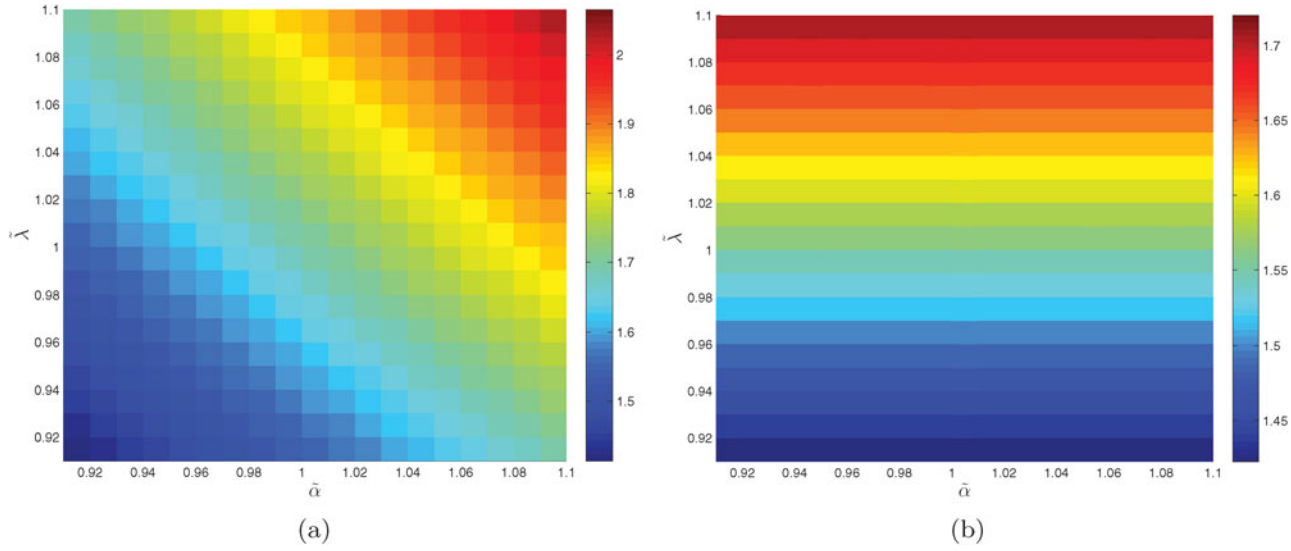

Figure 4. The left (a) and right (b) figures depict, respectively, the optimal amplitude and frequency computed with Equations (47) and (48) for many values of $\tilde{\boldsymbol{\theta}}_g$.

5.3 Identification results

In this section, we identify the physical parameters $\tilde{\boldsymbol{\theta}}_0$ with the optimal input signal computed in the previous section (49). We use method (2) as detailed in Section 3. The resulting unscaled data-set Z_N is defined by scaling (45) and the scaled sampled equivalent of the input (50). We remind the reader that we consider the case $x_u = x_y = 0$. The data-set $\tilde{Z}_N = \left\{\frac{u_D[j]}{u_s}, \frac{y_D[j]}{y_s}\right\}_{j=2001,\ldots,N}$, where u_s and y_s are defined in Section 5.1. Note that we discarded the first 2000 samples to remove transients. Simulation of the scaled noise-free output $\tilde{y}_{\mathrm{nf}}(\tilde{t})$ (43) is done according to Section 3.2.1 where we chose $\Delta\tilde{t} = T_s/t_s$ and $M = 200$. The simulated noise-free output $\tilde{y}_{\mathrm{sim}}[j]$ for $j = 2001, \ldots, N$ is then used together with the scaled measured data $y_D[j]/y_s$ in $\tilde{Z}_N$ in the least-squares procedure (9). For one experiment we found the scaled estimates resulting from this procedure to be $\hat{\tilde{\alpha}}_N = 1.01$ and $\hat{\tilde{\lambda}}_N = 1.005$, corresponding to unscaled estimates $\hat{\alpha}_N = 3.414 \times 10^{-5}$ $\mathrm{m^2 s^{-1}}$ and $\hat{\lambda}_N = 111.56$ $\mathrm{Wm^{-1}{}^{\circ}C^{-1}}$. These estimates fall within the respective intervals $[\lambda_0 - 0.01\lambda_0, \lambda_0 + 0.01\lambda_0]$ and $[\alpha_0 - 0.02\alpha_0, \alpha_0 + 0.02\alpha_0]$ that we set in Section 5.2.

5.3.1 Monte Carlo simulations experiment 1: validating the variance constraints

To validate whether the variance constraints are honoured, we ran 2×10^4 Monte Carlo simulations to identify the scaled physical parameters $\tilde{\alpha}_0 = 1$ and $\tilde{\lambda}_0 = 1$ with the optimal signal (49). (In other words, 20,000 data-sets Z_N were generated and for each the identification procedure was applied.) The identified parameters $\tilde{\alpha}_N$ and $\tilde{\lambda}_N$ for all experiments are shown in Figure 5. The mean value of the coordinate $\tilde{\boldsymbol{\theta}}_N = [\tilde{\alpha}_0, \tilde{\lambda}_0]$ is indicated by the red cross. The constraints set in Section 5.2 are visualised by the square resulting from intersection horizontal and vertical dashed black lines.

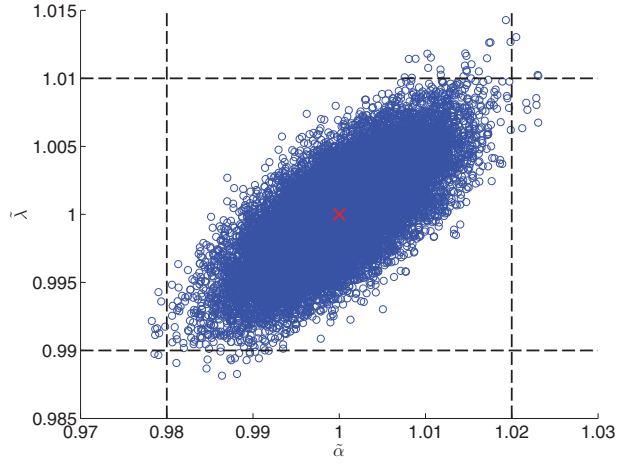

Figure 5. Twenty thousand identified vectors $\tilde{\theta}_N$ are indicated by the blue open circles, the mean value of $\tilde{\theta}_N$ over all Monte Carlo simulations by the red cross, and the constraints on the parameters $\tilde{\alpha}_N$ and $\tilde{\lambda}_N$ by the square generated through the intersection of the dashed black lines. Only 0.28% of the estimates lies outside the square.

Observe that almost none of the estimates $\tilde{\theta}_N$ lie outside the region of constraints. The computed variance for $\tilde{\alpha}_N$ and $\tilde{\lambda}_N$ are, respectively, $\mathrm{var}(\tilde{\alpha}_N) = 3.615 \times 10^{-5}$ and

$\text{var}(\tilde{\lambda}_N) = 1.1108 \times 10^{-5}$. Clearly, the optimal input signal designed in the previous section honours the constraints. The experiment design procedure ensured that the confidence ellipse 'touches' the horizontal constraints, whereas the variance in $\tilde{\alpha}_N$ is in fact a bit smaller. This is not surprising, as explained in Appendix 2.

Slightly lower accuracy in the estimates is obtained in Gabano and Poinot (2009) for the same experiment length N, parameters $\alpha_0$andλ_0, and rod length L. The input signal they considered was a pseudo-random binary excitation signal with a power distribution in the higher frequencies, up to 20 rads^{-1}. The amplitudes are of the same order but the noise variances might be different, so a comparison is difficult. However, independent of this difference, our result suggests that one should instead use a very low excitation frequency, i.e. 0.02 rad s^{-1} to get the most accurate estimates. As shown in Figure 4(b), choosing high frequencies leads to matrix $P_{\tilde{\theta}}^{-1}$ that is much smaller than using one that is close to the maxima of the derivatives. Intuitively, it means that the system is highly insensitive to high-frequency input signals.

Our results also suggest that higher accuracy can be obtained by measuring at $\tilde{x}_y = 0.12$ as shown in Figure 4(a). The ratio of the optimal amplitude between $\tilde{x}_y=0$ and $\tilde{x}_y = 0.12$ is 1.03. As $\tilde{P}_{\tilde{\theta}}^{-1}$ is proportional to $\tilde{A}^2$, it means that 1.03^2 higher accuracies can be obtained using the same input power.

5.3.2 Monte Carlo simulations experiment 2: chicken-and-egg problem revisited

In Section 4, we mentioned that OED suffers from the chicken-and-egg problem. In this section, we show that we can still find estimates that honour the user-imposed constraints, even if we do not know exactly $\tilde{\boldsymbol{\theta}}_0$.

To this end, suppose that we start without any prior knowledge on $\boldsymbol{\theta}_0$. We run an experiment of length $N/2$ and apply a white-noise input signal[8] with high variance $\tilde{\sigma}^2_{\text{wn}}=25$. This delivers us an estimate $\hat{\tilde{\boldsymbol{\theta}}}_{\text{wn}}$. At this point, we compare two scenarios: (1) we apply optimal experiment design to find the optimal input signal that guarantees the constraints (46) based on the initial guess $\tilde{\boldsymbol{\theta}}_g=\hat{\tilde{\boldsymbol{\theta}}}_{\text{wn}}$ for an experiment length of $N/2$, or (2) continue with applying a white-noise signal that has the same power as the optimal input signal and equal experiment length. Both scenarios thus have equally powered input signals and the experiments have equal length.

Using Monte Carlo simulations, we first generate 500 white-noise realisation with variance $\tilde{\sigma}^2_{\text{wn}}=25$ that generate 500 estimates $\hat{\tilde{\boldsymbol{\theta}}}_{\text{wn}}$, which we collect in the set $\{\hat{\tilde{\theta}}_{\text{wn}}\}$. These estimates are shown in red in Figure 6. Next, for each of the estimates, we run scenarios (1) and (2). The estimates

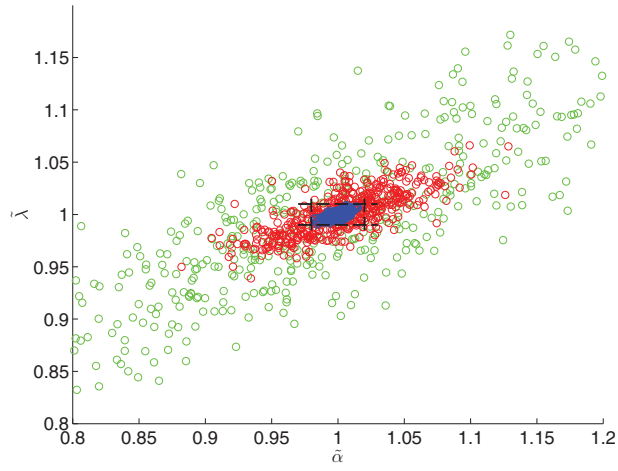

Figure 6. Monte Carlo simulations. The red, blue and green circles correspond to the set of initial guesses $\{\hat{\tilde{\theta}}_{\text{wn}}\}$, estimates generated by optimal input signals and estimates from white-noise input signals with a power that is equal to their respective optimal input signal.

resulting from scenarios (1) and (2) are shown in blue and green in Figure 6, respectively. We find that the variances of the estimates in scenario (1) are $\text{var}(\hat{\tilde{\alpha}}_{N/2})=3.1381\times10^{-5}$ and $\text{var}(\hat{\tilde{\lambda}}_{N/2}) = 9.2074 \times 10^{-6}$, which are both smaller than the required variances of respectively 4.44×10^{-5} and 1.11×10^{-5}. The equally powered white noise realisations of scenario (2) deliver much worse estimates.

Since both scenarios generate signals that are equally long and equally powered, these Monte Carlo simulations clearly illustrate the advantage of optimal experiment design.

The above approach is the classical approach to tackle the chicken-and-egg problem. More involved approaches exist. In these approaches, the initial guess and the optimal spectrum are adapted throughout the experiment (see e.g. Forgione, Bombois, & Van den Hof, 2013; Gerencsèr, Hjalmarsson, & Mårtensson, 2009; Larsson et al., 2013).

6. Conclusions

The main novelty of this paper is the introduction of a systematic way to identify physical parameters in linear physical systems in a least intrusive manner while guaranteeing accuracy on the to-be-identified parameters. We have in particular shown how to apply the theory of least costly experiment design to diffusion–advection processes.

To this end, we made use of a discretisation using the Crank–Nicolson stencil to truncate the continuous-time model to find a discrete-time transfer function that

couples the input and output. This transfer function is then also guaranteed to be stable. This integration scheme is not only unconditionally stable, but also more accurate than the Euler stencil. The resulting truncated model is a state-space realisation that is explicit in the physical parameters. We then showed how optimal experiment design can be applied.

The second novelty of this paper is the generalisation of the experiment design framework to find not only optimal amplitudes and frequencies, but also optimal actuator and sensor locations.

We applied our methodology to the estimation of two thermal parameters in a front-face experiment. This study showed that current practice, i.e. placing the sensor and actuator at position $x = 0$, in fact does not deliver the best possible estimates. Our study suggests that placing the sensor location at a distance of 12% of the total length of the rod from the actuator position yields estimates that are 6% better. Applying the optimal input signals designed in the case study furthermore shows that the input power can be reduced considerably in comparison to previous experiments.

It is interesting to extend the methodology to physical systems with spatially dependent parameters. This is considered to be future work.

Notes

1. For a general introduction to optimal experiment design, we refer the reader to the nice historical review of Mehra (1974).
2. For simplicity, we considered only one spatial dimension, but more can be incorporated easily.
3. The scaling procedure explained here is classical, except that usually in the literature the parameters are (assumed to be) known. In such cases, one can make most terms equal to unity in step (4), rather than of $O(1)$.
4. The simulation accuracy is thus $O(\Delta\tilde{t})^2$. If $\Delta\tilde{t}$ turns out to be large, define the integer γ such that the time integration step becomes $\Delta\tilde{t}/\gamma$. This generates γ times more points in the considered simulation time interval. In the identification procedure, one then has to downsample the simulated output by a factor γ.
5. Since the Nyquist frequency is chosen a decade above the system's bandwidth it is generally not necessary to cover the whole frequency range $[0, \pi/Ts]$
6. If $x_u = 0$, we can easily heat the cross-sectional area. If x_u 0, the rod can be heated locally with a thin thermal band wrapped around the rod.
7. This optimal input signal has a different optimal frequency than the case $\tilde{x}_y = 0.12$.
8. Note that we now can only use identification method (2) of Section 3, because the input signal is no longer periodic, whereas in Experiment 1 we could have also opted for method (1) since the input signal is periodic and a closed-form transfer function exists.

Acknowledgments

The authors acknowledge Prof. Rashtchian of Sharif University of Technology, Iran, for supporting the assignment of M. Mansoori to TU Delft.

Disclosure statement

No potential conflict of interest was reported by the authors.

References

Aoun, M., Malti, R., Levron, F., & Oustaloup, A. (2004). Numerical simulations for fractional systems: An overview of existing methods and improvements. *Nonlinear Dynamics, 38*, 117–131.

Bombois, X., Scorletti, G., Van den Hof, P.M.J., & Hildebrand, R. (2006). Least-costly identification experiment for control. *Automatica, 42*, 1651–1662.

Didierjean, S., Maillet, D., & Moyne, C. (2004). Analytical solutions of one-dimensional macrodispersion in stratisfied porous media by the quadrupole method: Convergence to an equivalent homogenous porous medium. *Advances in Water Resources, 27*, 657–667.

Forgione, M., Bombois, X., & Van den Hof, P.M.J. (2013). Experiment design for batch-to-batch model-based learning control. In *Proceedings of the 2013 American Control Conference* (pp. 3912–3917). Washington DC: IEEE.

Gabano, J.-D., & Poinot, T. (2009). Fractional modelling applied to heat conductivity and diffusivity estimation. *Physica Scripta, 136*, 1–6.

Gabano, J.-D., & Poinot, T. (2011). Fractional modelling and identification of thermal systems. *Signal Processing, 91*, 531–541.

Gerencsèr, L., Hjalmarsson, H., & Mårtensson, J. (2009). Identification of ARX systems with non-stationary inputs - Asymptotic analysis with applications to adaptive input design. *Automatica, 45*, 623–633.

Grant, M., & Boyd, S. (2013). CVX: Matlab software for disciplined convex programming. http://cvxr.com/cvx

Jansson, H., & Hjalmarsson, H. (2005). Input design via LMIs admitting frequency-wise model specifications in confidence regions. *IEEE Transactions on Automatic Control, 50*(10), 1534–1549.

Larsson, C.A., Annergren, M., Hjalmarsson, H., Rojas, C.R., Bombois, X., Mesbah, A., & Modèn, P.E. (2013). Model predictive control with integrated experiment design for OE systems. In *Proceedings of the 2013 European Control Conference* (pp. 3790–3795). Zurich, Switzerland: IEEE.

Ljung, L. (1999). *System identification: Theory for the user*. Englewood Cliffs, NJ: Prentice Hall.

Manchester, I.R. (2009). An algorithm for amplitude-constrained input design for system identification. In *Proceedings of the 48th IEEE Conference on Decision and Control* (pp. 1551–1556). Shanghai: IEEE.

Mansoori, M., Van den Hof, P.M.J., Janssen, J.D., & Rashtchian, D. (2014). Pressure transient analysis of bottomhole pressure and rate measurements using system identification techniques. *SPE Journal, SPE-176031-PA*.

Mehra, R.K. (1974). Optimal input signals for parameter estimation in dynamic systems – survey and new results. *IEEE Transactions on Automatic Control, 19*(6), 753–768.

Pintelon, R., Schoukens, J., Pauwels, L., & van Gheem, E. (2005). Diffusion systems: Stability, modeling, and identification. *IEEE Transactions on Instrumentation and Measurement, 54*(5) 2061–2067.

Point, T., & Trigeassou, J. (2003). A method for modelling and simulation of fractional systems. *Signal Processing, 83*, 2319–2333.

Point, T., Trigeassou, J., & Lin, J. (2002) (pp. 462–468). Barcelona, Spain: IFAC. Parameter estimation of fractional models: Application to modeling of diffusive systems. In *15th Triennial World Congress 2002* (pp. 462–468). Barcelona, Spain: IFAC.

Potters, M.G., Forgione, M., Bombois, X., & van den Hof, P.M.J. (2015). Least-costly experiment design for uni-parametric linear models: An analytical approach. In *the Proceedings of the 2015 European Control Conference* (pp. 848–853). Linz: IEEE.

Rensfelt, A., Mousavi, S., Mossberg, M., & Söderström, T. (2008). Optimal sensor locations for non-parametric identification of viscoelastic materials. *Automatica, 44*, 28–38.

Schorsch, J., Garnier, H., Gilson, M., & Young, P. (2013). Instrumental variable methods for identifying partial differential equation models. *International Journal of Control, 86*(12), 2325–2335.

Thomas, L.H. (1949). *Elliptic problems in linear differential equations over a network*. Watson Scientific Computing Laboratory Report. New York City, NY: Columbia University.

Uciński, D. (2004). *Optimal measurement methods for distributed parameter system identification*. Florida: CRC Press.

Wagner, B.J., & Harvey, J.W. (1997). Experiment design for estimating parameters of rate-limited mass transfer: Analysis of stream tracer studies. *Water Resources Research, 33*(7), 1731–1741.

Yeh, W. (1986). Review of parameter identification procedures in groundwater hydrology: The inverse problem. *Water Resources Research, 22*(2), 96–118.

Appendix 1. Derivation of continuous-time transfer function of 1D diffusion equation

We consider the 1D problem of a diffusion process on a line with domain $\mathcal{D} = [0, L]$. The physical parameters are collected in the vector $\boldsymbol{\theta} = [\theta_1, \theta_2]$. The problem is defined by

$$\frac{\partial f(x,t)}{\partial t} = \theta_1 \frac{\partial^2 f(x,t)}{\partial x^2} \tag{A1}$$

subject to the boundary conditions

$$\phi(x,t) = -\theta_2 \frac{\partial f(x,t)}{\partial x}, \quad f(L,t) = 0 \,\forall t. \tag{A2}$$

We define the input of the system by $u(t) = \phi(x_u, t)$ and the output $y_{\text{nf}}(t) = f(x_y, t)$, where $x_u, x_y \in \mathcal{D}$ denote the input and output locations on the line. To solve the problem, we first apply the Laplace transform to the above equations:

$$sF(x,s) = \theta_1 \frac{\partial^2 F(x,s)}{\partial x^2} \tag{A3}$$

$$\Phi(x,s) = -\theta_2 \frac{\partial F(x,s)}{\partial x}. \tag{A4}$$

The general solution to Equation (A3) reads

$$F(x,s) = c_1 e^{\sqrt{\frac{s}{\theta_1}}x} + c_2 e^{-\sqrt{\frac{s}{\theta_1}}}, \tag{A5}$$

where c_1 and c_2 are real constants that will be determined from the boundary conditions. From this equation, it follows that Equation (A4) becomes

$$\Phi(x,s) = -\theta_2 \sqrt{\frac{s}{\theta_1}} \left\{ c_1 e^{\sqrt{\frac{s}{\theta_1}}x} - c_2 e^{-\sqrt{\frac{s}{\theta_1}}x} \right\}. \tag{A6}$$

We also have that the input and output in the Laplace domain read $U(s) = \Phi(x_u, s)$ and $Y_{\text{nf}}(s) = F(x_y, s)$. We can thus write

$$U(s) = \Phi(x_u, s) = -\theta_2 \sqrt{\frac{s}{\theta_1}} \left\{ c_1 e^{\sqrt{\frac{s}{\theta_1}}x_u} - c_2 e^{-\sqrt{\frac{s}{\theta_1}}x_u} \right\} \tag{A7}$$

from which follows that

$$c_1 = e^{-\sqrt{\frac{s}{\theta_1}}x_u} \left\{ -\frac{1}{\theta_2}\sqrt{\frac{s}{\theta_1}} U(s) + c_2 e^{-\sqrt{\frac{s}{\theta_1}}x_u} \right\}. \tag{A8}$$

Furthermore, from Equation (A5) and the boundary condition $F(L, s) = 0 \;\forall s$, we get

$$F(L,s) = c_1 e^{\sqrt{\frac{s}{\theta_1}}L} + c_2 e^{-\sqrt{\frac{s}{\theta_1}}L} = 0 \;\rightarrow\; c_2 = -c_1 e^{2\sqrt{\frac{s}{\theta_1}}L}. \tag{A9}$$

We can now combine Equations (A8) and (A9) to find that

$$c_1 = -\frac{1}{\theta_2}\sqrt{\frac{\theta_1}{s}} \frac{e^{-\sqrt{\frac{s}{\theta_1}}x_u}}{1 + e^{2\sqrt{\frac{s}{\theta_1}}(L-x_u)}} U(s), \tag{A10}$$

$$c_2 = \frac{1}{\theta_2}\sqrt{\frac{\theta_1}{s}} \frac{e^{-\sqrt{\frac{s}{\theta_1}}(x_u-2L)}}{1 + e^{2\sqrt{\frac{s}{\theta_1}}(L-x_u)}} U(s). \tag{A11}$$

Next, we can write the expression for $Y_{\text{nf}}(s) = F(x_y, s)$ which reads

$$Y_{\text{nf}}(s) = c_1 e^{\sqrt{\frac{s}{\theta_1}}x_y} + c_2 e^{-\sqrt{\frac{s}{\theta_1}}x_y} \tag{A12}$$

$$= -\frac{1}{\theta_2}\sqrt{\frac{\theta_1}{s}} \frac{e^{-\sqrt{\frac{s}{\theta_1}}(x_u-x_y)}}{1 + e^{2\sqrt{\frac{s}{\theta_1}}(L-x_u)}} \left\{ 1 - e^{2\sqrt{\frac{s}{\theta_1}}(L-x_y)} \right\} U(s). \tag{A13}$$

Hence, the transfer function between input and output reads

$$G_{x_u,x_y}(s,\boldsymbol{\theta}) = \frac{Y_{\text{nf}}(s)}{U(s)} = -\frac{1}{\theta_2}\sqrt{\frac{\theta_1}{s}}\frac{e^{-\sqrt{\frac{s}{\theta_1}}(x_u-x_y)}}{1+e^{2\sqrt{\frac{s}{\theta_1}}(L-x_u)}}\left\{1-e^{2\sqrt{\frac{s}{\theta_1}}(L-x_y)}\right\}, \tag{A14}$$

which can be further simplified to

$$G_{x_u,x_y}(s,\boldsymbol{\theta}) = \frac{1}{\theta_2}\sqrt{\frac{\theta_1}{s}}\frac{\sinh\left[\sqrt{\frac{s}{\theta_1}}(L-x_y)\right]}{\cosh\left[\sqrt{\frac{s}{\theta_1}}(L-x_u)\right]}. \tag{A15}$$

Substitution of $f(x,\ t) = T(x,\ t)$ in Equation (A1) and following the same calculations yields the equation above. Finally, setting $\theta_1 = \alpha_0$ and $\theta_2 = \lambda_0$ results in $G_{x_u,x_y}(s,\boldsymbol{\theta}_0)$, in which $\boldsymbol{\theta}_0 = [\alpha_0, \lambda_0]$. In a similar fashion, the continuous-time transfer function between the scaled input and scaled output can be derived for Equations (42) and (43), yielding

$$\tilde{G}_{\tilde{x}_u,\tilde{x}_y}(\tilde{s},\tilde{\boldsymbol{\theta}}) = \frac{1}{\tilde{\theta}_2}\sqrt{\frac{\tilde{\theta}_1}{\tilde{s}}}\frac{\sinh\left[\sqrt{\frac{\tilde{s}}{\tilde{\theta}_1}}(1-\tilde{x}_y)\right]}{\cosh\left[\sqrt{\frac{\tilde{s}}{\tilde{\theta}_1}}(1-\tilde{x}_u)\right]}. \tag{A16}$$

This equation is equal to (44) after substitution of $\tilde{\boldsymbol{\theta}} = \tilde{\boldsymbol{\theta}}_0 = [\tilde{\alpha}_0, \tilde{\lambda}_0]$.

Appendix 2. An analytical solution to the 2D least costly experiment design problem

This section derives the analytical solution of the optimal input signal that is found numerically in Section 5. The derivation here is not specific to this example, but is a general solution for systems of which two parameters need to be identified. In this appendix, we have dropped all tildes on variables and parameters to simplify notation.

Our starting point is the problem definition introduced in Section 4. In the particular case if identifying two parameters $\boldsymbol{\theta}_0$ we require that the joint confidence region defined by the ellipse

$$(\boldsymbol{\theta}-\boldsymbol{\theta}_0)^T\boldsymbol{P}_\theta^{-1}[\Phi_u(\omega)](\boldsymbol{\theta}-\boldsymbol{\theta}_0) \le \chi^2_\alpha(2), \tag{B1}$$

in which $\chi^2_\alpha(2)$ is the α-quantile of the chi-squared distribution, lies inside the intervals

$$i = 1, 2: \ -\Delta\theta_i + \theta_{0,i} \le \hat{\theta}_0 \le \Delta\theta_i + \theta_{0,i}. \tag{B2}$$

Furthermore, we not only require these constraints to hold, but also to find the spectrum in Equation (B1) that minimises the cost as given in Equation (29). This constraint is equivalent to the variance constraint (27).

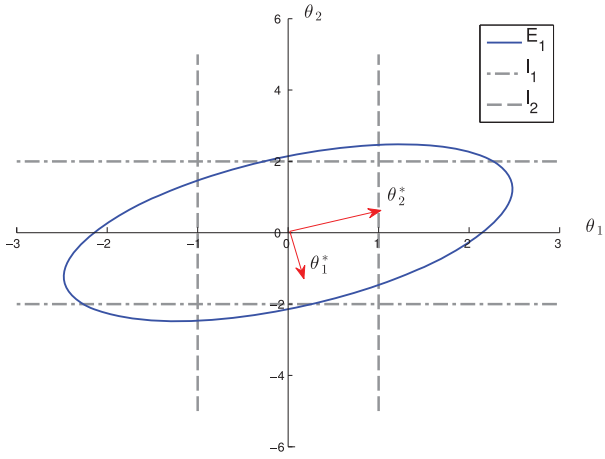

Figure B1. The blue ellipse E_1 corresponds to the boundary of the confidence region $\boldsymbol{\theta}^T\boldsymbol{P}_\theta^{-1}\boldsymbol{\theta} \le \chi^2_\alpha(2)$. The dashed and dash–dotted grey line sets correspond to the constraints on parameter θ_1 and θ_2, respectively.

The situation is sketched in Figure B1. The blue ellipse E_1 is described by Equation (B1), the sets of horizontal and vertical lines l_1 and l_2 indicate the intervals given in Equation (B2). The goal is now to find the spectrum $\Phi_u(\omega)$ that minimises the cost, while at the same time ensuring that the ellipse E_1 lies inside the box defined by the four intersection points of the sets of lines. To keep notation ease, we translated the centre of the ellipse from $\boldsymbol{\theta}_0$ to (0, 0) without loss of generality.

We recall that we parameterise the spectrum as a multi-sine. It is known in System Identification that two parameters can be identified with a single sine. In this appendix, we give the solution to the optimisation problem defined in Section 4 assuming the solution lies in the family of single sines. The optimisation problem thus reads

$$\min_A \frac{1}{2}A^2 \tag{B3}$$

subject to the constraints

$$\forall\boldsymbol{\theta} = (\theta_1,\theta_2) \text{ for which } \boldsymbol{\theta}^T\boldsymbol{P}_\theta^{-1}[A]\boldsymbol{\theta} = \chi^2_\alpha(2) : |\theta_1| \le |\Delta\theta_1|, \text{ and } |\theta_2| \le |\Delta\theta_2| \tag{B4}$$

in which

$$\boldsymbol{P}_{\boldsymbol{\theta}}^{-1}[A] = \frac{NA^2}{2\sigma_e^2}\text{Re}\left\{\left[\frac{\partial G_{i_u,i_y}(e^{i\omega T_s},\boldsymbol{\theta})}{\partial\boldsymbol{\theta}}\right]_{\boldsymbol{\theta}=\boldsymbol{\theta}_0} \times \left[\frac{\partial G_{i_u,i_y}(e^{-i\omega T_s},\boldsymbol{\theta})}{\partial\boldsymbol{\theta}}\right]^T_{\boldsymbol{\theta}=\boldsymbol{\theta}_0}\right\}. \tag{B5}$$

Theorem B.1: *The solution to optimisation problem (B3)-(B4) is given by the optimal input signal*

$$u_{opt}(t) = A_{opt}\cos(\omega_{opt}t + \phi), \tag{B6}$$

in which ϕ is an arbitrary phase,

$$A_{opt} = \max\left\{\min_{\omega} A_1(\omega), \min_{\omega} A_2(\omega)\right\}, \tag{B7}$$

and, if we denote i_{opt} as the index that corresponds to the function A_i which has the highest minimum between the functions $A_1(\omega)$ and $A_2(\omega)$,

$$\omega_{opt} = \arg\min_{\omega} A_{i_{opt}}(\omega), \tag{B8}$$

and lastly, for $i = 1, 2$,

$$A_i(\omega) = \sqrt{\left[\frac{d_2(\omega)}{D_{i,2}(\omega)}\right]^2 + \left[\frac{d_1(\omega)}{D_{i,1}(\omega)}\right]^2}, \tag{B9}$$

$$m_1 = \frac{||\boldsymbol{v}_1(\omega)||}{||\boldsymbol{v}_2(\omega)||}\frac{\lambda_2(\omega) - p_{22}(\omega)}{\lambda_1(\omega) - p_{22}(\omega)},\ m_2 = \frac{||\boldsymbol{v}_1(\omega)||}{||\boldsymbol{v}_2(\omega)||}, \tag{B10}$$

$$b_1(\omega) = \frac{|\Delta\theta_1|}{||\boldsymbol{v}_2(\omega)||}p_{12}(\omega)\left[1 - \frac{\lambda_2(\omega) - p_{22}(\omega)}{\lambda_1(\omega) - p_{22}(\omega)}\right],$$
$$b_2(\omega) = \frac{|\Delta\theta_2|}{||\boldsymbol{v}_2(\omega)||}[\lambda_2(\omega) - \lambda_1(\omega)], \tag{B11}$$

$$d_i(\omega) = \sqrt{\chi^2_\alpha(2)/\lambda_i(\omega)},\ D_{i,1}(\omega) = -b_i(\omega)/m_i(\omega),$$
$$D_{i,2}(\omega) = b_i(\omega), \tag{B12}$$

$$||\boldsymbol{v}_i(\omega)|| = \sqrt{p_{12}^2(\omega) + (\lambda_i(\omega) - p_{22}(\omega))^2}, \tag{B13}$$

(B14)

where $\lambda_1(\omega)$ and $\lambda_2(\omega)$ are, respectively, the largest and smallest eigenvalue of matrix $\boldsymbol{P}$ given by

$$\boldsymbol{P} = Re\left\{\begin{pmatrix} p_{11}(\omega) & p_{12}(\omega) \\ p_{12}(\omega) & p_{22}(\omega)\end{pmatrix}\right\}, \tag{B15}$$

with the elements

$$p_{11}(\omega) = \frac{N}{2\sigma_e^2}\left|\frac{\partial G(e^{-i\omega T_s}, \boldsymbol{\theta})}{\partial\theta_1}\right|^2_{\theta=\theta_1}, \tag{B16}$$

$$p_{12}(\omega) = \frac{N}{2\sigma_e^2}\left[\frac{\partial G(e^{-i\omega T_s}, \boldsymbol{\theta})}{\partial\theta}\right]_{\theta=\theta_1}\left[\frac{\partial G(e^{i\omega T_s}, \boldsymbol{\theta})}{\partial\theta}\right]_{\theta=\theta_2}, \tag{B17}$$

$$p_{22}(\omega) = \frac{N}{2\sigma_e^2}\left|\frac{\partial G(e^{-i\omega T_s}, \boldsymbol{\theta})}{\partial\theta_2}\right|^2_{\theta=\theta_2}. \tag{B18}$$

Proof. We consider the positive quarter of the plane (θ_1, θ_2) in Figure B1. The first part of the proof consists of the observation that to obtain the optimal input signal, it should hold that the ellipse E_1 is tangent to either line l_1 or l_2, as depicted in Figure B1. Indeed, if the ellipse is not tangent to one of these lines, then either (1) the ellipse exceeds the constraints, or (2) the ellipse lies completely inside the rectangle and has no intersection point with the lines. In case (1), we trivially see that we find no solution, whereas in case (2), the amplitude A that scales the confidence ellipse (B1) is larger than necessary, and the solution is thus not optimal.

The proof now proceeds as follows. First, we find all amplitudes $A_1(\omega)$ and $A_2(\omega)$ such that ellipse E_1 is tangent to, respectively, line l_1 and l_2. Once we have these functions, we find the frequencies that minimise $A_1(\omega)$ and $A_2(\omega)$. The optimal amplitude will then correspond to the largest of the two minima, since this amplitude corresponds to the most stringent constraint. (We then ensure that the ellipse lies within both set of lines.)

To this end, we apply a coordinate transformation from $\boldsymbol{\theta} \to \boldsymbol{\theta}^*$ as to align our coordinate system with the principal axes of ellipse E_1. The new coordinate system is shown in red in Figure B1 and is spanned by the eigenvectors of matrix $\boldsymbol{P}_\theta^{-1}$. Let us write $\boldsymbol{P}_\theta^{-1}$ as

$$\boldsymbol{P}_\theta^{-1} = A^2\boldsymbol{P}. \tag{B19}$$

The eigenvalues of $\boldsymbol{P}$ are given by

$$\lambda_{1,2} = \frac{1}{2}\mathrm{Tr}[\boldsymbol{P}] \pm \frac{1}{2}\sqrt{\mathrm{Tr}^2[\boldsymbol{P}] - 4\det[\boldsymbol{P}]} \tag{B20}$$

and its normalised eigenvectors by

$$\boldsymbol{u}_1 = \frac{1}{||\boldsymbol{v}_1||}\begin{pmatrix}\lambda_1 - p_{22} \\ p_{12}\end{pmatrix}, \tag{B21}$$

$$\boldsymbol{u}_2 = \frac{1}{||\boldsymbol{v}_2||}\begin{pmatrix}\lambda_2 - p_{22} \\ p_{12}\end{pmatrix}, \tag{B22}$$

(B23)

in which $||\boldsymbol{v}_i|| = \sqrt{p_{12}^2 + (\lambda_i - p_{22})^2}$ for $i = 1, 2$. We define the coordinate transformation via $\boldsymbol{\theta} = \boldsymbol{M}\boldsymbol{\theta}^*$. If we choose the matrix $\boldsymbol{M}$ as

$$\boldsymbol{M} = \begin{pmatrix}\boldsymbol{u}_1 & \boldsymbol{u}_2\end{pmatrix}, \tag{B24}$$

then ellipse E_1 can be rewritten as

$$\boldsymbol{\theta}^T\boldsymbol{P}_\theta^{-1}\boldsymbol{\theta} = (\boldsymbol{M}\boldsymbol{\theta}^*)^T A^2\boldsymbol{P}(\boldsymbol{M}\boldsymbol{\theta}^*) = A^2\boldsymbol{\theta}^*\boldsymbol{M}^T\boldsymbol{P}\boldsymbol{M}\boldsymbol{\theta}^*$$
$$= A^2\boldsymbol{\theta}^*\boldsymbol{D}\boldsymbol{\theta}^* = \chi^2_\alpha(2), \tag{B25}$$

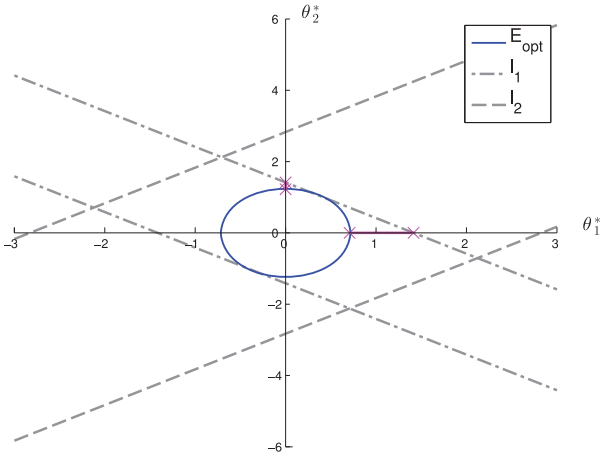

Figure B2. The same situation as in Figure B1 but now in the new coordinate frame (θ_1^*, θ_2^*).

where $\boldsymbol{D} = \boldsymbol{M}^T\boldsymbol{P}\boldsymbol{M}$ is, by construction, a diagonal matrix containing the eigenvalues $\lambda_{1,2}$. In the new coordinate system $\boldsymbol{\theta}^*$, the principal axes are thus aligned with the coordinate axes (see Figure B2).

The second step is to find expressions for the lines l_1 and l_2 in Figure B1 in the new reference frame. We can consider the lines in the upper right quadrant in Figure B1. Line l_1 is given by $\theta_2 = \Delta\theta_2\ \forall\theta_1$ and line l_2 by $\theta_1 = \Delta\theta_1\ \forall\theta_2$. We choose two arbitrary points on l_1 and denote them by $Z_{1,1} = (0, \Delta\theta_1)$ and $Z_{1,2} = (\Delta\theta_1, \Delta\theta_1)$. Similarly, for line l_2 we define $Z_{2,1} = (\Delta\theta_2, 0)$ and $Z_{2,2} = (\Delta\theta_2, \Delta\theta_2)$. Then, using the transformation $\boldsymbol{\theta}^* = \boldsymbol{M}^T\boldsymbol{\theta}$,

$$\begin{pmatrix}\theta_1^*\\ \theta_2^*\end{pmatrix} = \begin{pmatrix}\frac{\lambda_1 - p_{22}}{||\boldsymbol{v}_1||} & \frac{p_{12}}{||\boldsymbol{v}_1||}\\ \frac{\lambda_2 - p_{22}}{||\boldsymbol{v}_2||} & \frac{p_{12}}{||\boldsymbol{v}_2||}\end{pmatrix}\begin{pmatrix}\theta_1\\ \theta_2,\end{pmatrix} \tag{B26}$$

we can find the new lines $l_i^* : \theta_2^* = m_i\theta_1^* + b_i$ for $i = 1, 2$. The slope m_i can be found by substituting the points $Z_{i,1}$ and $Z_{i,2}$ into the above equations and calculating $m_i = \frac{\Delta\theta_2^*}{\Delta\theta_1^*}$. The offset b_i can then be calculated trivially. The result is

$$l_1^* :\ \theta_2^* = m_1\theta_1^* + b_1 = \frac{||v_1||}{||v_2||}\frac{\lambda_2 - p_{22}}{\lambda_1 - p_{22}}\theta_1^* + \frac{\Delta\theta_1}{||v_2||}p_{12}\left[1 - \frac{\lambda_2 - p_{22}}{\lambda_1 - p_{22}}\right], \tag{B27}$$

$$l_2^* :\ \theta_2^* = m_2\theta_1^* + b_2 = \frac{||v_1||}{||v_2||}\theta_1^* + \frac{\Delta\theta_2}{||v_2||}\left[\lambda_2 - \lambda_1\right]. \tag{B28}$$

The result of these transformations are shown in Figure B2.

The final step is to find the condition for internal tangency of the ellipse with both lines l_1^* and l_2^*. The ellipse in the new coordinate system is given by

$$E_1^* : \boldsymbol{\theta}^{*T}\boldsymbol{D}\boldsymbol{\theta}^* = \lambda_1\theta_1^{*2} + \lambda_2\theta_2^{*2} = \chi_\alpha^2(2)/A^2. \tag{B29}$$

Substitution of line l_i^* into the above equation and rearranging terms yields

$$(\lambda_1 + m_i^2\lambda_2)\theta_1^{*2} + 2\lambda_2 m_i b_i\theta_1^* + \lambda_2 b_i^2 - \chi_\alpha^2(2)/A^2 = 0. \tag{B30}$$

This is a quadratic equation in θ_1^* which has as solutions

$$\theta_{1,\pm}^* = -\frac{2\lambda_2 m_i b_i}{2(\lambda_1 + m_i^2\lambda_2)} \pm \frac{1}{\lambda_1 + m_i^2\lambda_2} \times \sqrt{\lambda_2^2 m_i^2 b_i^2 - \left(\lambda_1 + m_i^2\lambda_2\right)\left(\lambda_2 b_i^2 - \chi_\alpha^2(2)/A^2\right)}. \tag{B31}$$

If ellipse E_1^* is tangent to line l_i^*, then only one point of intersection exists. This means that the discriminant in the above equation should be equal to zero. Hence, we have the condition

$$\lambda_2^2 m_i^2 b_i^2 = (\lambda_1 + m_i^2\lambda_2)(\lambda_2 b_i^2 - \chi_\alpha^2(2)/A_i^2), \tag{B32}$$

where A_i is the amplitude we seek such that the above equality holds for line l_i. Rearranging the above equation yields the solutions

$$A_i^2(\omega) = \frac{\chi_\alpha^2(2)}{b_i^2(\omega)}\left[\lambda_2(\omega) - \frac{\lambda_2^2(\omega)m_i^2(\omega)}{\lambda_1(\omega) + m_i^2(\omega)\lambda_2(\omega)}\right]^{-1}. \tag{B33}$$

In the last equation, we show the arguments of each function explicitly to indicate that they depend on the frequency. From (B29), we see that the lengths of the principal axes are given by $d_1(\omega) = \sqrt{\chi_\alpha^2(2)/\lambda_1(\omega)}$ and $d_2(\omega) = \sqrt{\chi_\alpha^2(2)/\lambda_2(\omega)}$. These points are indicated in Figure B2 by the first magenta crosses measured from the origin. Furthermore, the distance from the origin to the intersection of line l_i^* with the θ_1^* and θ_2^* axis is given by, respectively, $D_{i,1}(\omega) = -b_i(\omega)/m_i(\omega)$ and $D_{i,2}(\omega) = b_i(\omega)$.

Rewriting Equation (B33) as

$$A_i(\omega) = \sqrt{\chi_\alpha^2(2)}\sqrt{\frac{1}{b_i^2(\omega)\lambda_2} + \frac{1}{\lambda_1(\omega)b_i^2(\omega)/m_i^2(\omega)}} \tag{B34}$$

and substituting the expressions for d_1, d_2, D_i, D_2 into this equation results in

$$A_i(\omega) = \sqrt{\left[\frac{d_2(\omega)}{D_{i,2}(\omega)}\right]^2 + \left[\frac{d_1(\omega)}{D_{i,1}(\omega)}\right]^2}. \tag{B35}$$

We now have an expression for the amplitudes A_i such that ellipse E_1 touches line l_i^*. The optimal amplitude is thus given by

$$A_{\text{opt}} = \max\left\{\min_{\omega} A_1(\omega), \min_{\omega} A_2(\omega)\right\} \tag{B36}$$

and, if we denote i_{opt} as the index that corresponds to the function A_i which has the largest minimum between the functions $A_1(\omega)$ and $A_2(\omega)$,

$$\omega_{\text{opt}} = \arg\min_{\omega} A_{i_{\text{opt}}}(\omega). \tag{B37}$$

□

This is quite a remarkable result! It shows that the minimum amplitude corresponds to the situation in where the sum of amplification factors $d_1/D_{i,1}$ and $d_2/D_{i,2}$ is minimal. Stated differently, the lengths indicated in Figure B2 by magenta lines should be made as small as possible.

Appendix 3. Computation of the gradient $\partial G_{i_u,i_y}/\partial\theta$

In this appendix, we show how to compute the gradient $\partial G_{i_u,i_y}/\partial\boldsymbol{\theta}$ in Equation (34) evaluated at $\boldsymbol{\theta} = \boldsymbol{\theta}_0$ for given i_u, i_y. We start from Equation (34), which we here recall for convenience:

$$G_{i_u,i_y}(z,\boldsymbol{\theta}) = \boldsymbol{C}\left[z\boldsymbol{I} - \boldsymbol{A}(\boldsymbol{\theta})\right]^{-1}\boldsymbol{B}(\boldsymbol{\theta}). \tag{C1}$$

In this equation, $\boldsymbol{I}$ is the $(M+1)\times(M+1)$ identity matrix, $\boldsymbol{A}(\boldsymbol{\theta}) = \boldsymbol{\mathcal{E}}^{-1}\boldsymbol{\mathcal{A}}$, $\boldsymbol{B}(\boldsymbol{\theta}) = \boldsymbol{\mathcal{E}}^{-1}\boldsymbol{\mathcal{B}}(1+z)$, and $\boldsymbol{C} = \boldsymbol{\mathcal{C}}$. Here, $z = e^{i\omega T_s}$ and $\boldsymbol{\mathcal{E}}$, $\boldsymbol{\mathcal{A}}$, $\boldsymbol{\mathcal{B}}$, and $\boldsymbol{\mathcal{C}}$ are given by Equations (18) and (19).

Making use of the identities $\frac{\partial \boldsymbol{U}^{-1}}{\partial x} = -\boldsymbol{U}^{-1}\frac{\partial \boldsymbol{U}}{\partial x}\boldsymbol{U}^{-1}$ and $\frac{\partial(\boldsymbol{U}\boldsymbol{V})}{\partial x} = \boldsymbol{U}\frac{\partial \boldsymbol{V}}{\partial x} + \frac{\partial \boldsymbol{U}}{\partial x}\boldsymbol{V}$, where $\boldsymbol{U}, \boldsymbol{V}$ equally sized matrices and x a scalar, we find that the derivative of Equation (C1) with respect to parameter $\boldsymbol{\theta}_i$ reads

$$\frac{\partial G_{i_u,i_y}(z,\boldsymbol{\theta})}{\partial \boldsymbol{\theta}_i} = \boldsymbol{C}\left[z\boldsymbol{I} - \boldsymbol{A}(\boldsymbol{\theta})\right]^{-1} \times \left\{\frac{\partial \boldsymbol{B}(\boldsymbol{\theta})}{\partial \boldsymbol{\theta}_i} + \frac{\partial \boldsymbol{A}(\boldsymbol{\theta})}{\partial \boldsymbol{\theta}_i}\left[z\boldsymbol{I} - \boldsymbol{A}(\boldsymbol{\theta})\right]^{-1}\boldsymbol{B}(\boldsymbol{\theta})\right\}. \tag{C2}$$

The derivatives of $\boldsymbol{A}(\boldsymbol{\theta}) = \boldsymbol{\mathcal{E}}^{-1}(\boldsymbol{\theta})\boldsymbol{\mathcal{A}}(\boldsymbol{\theta})$ and $\boldsymbol{B}(\boldsymbol{\theta}) = \boldsymbol{\mathcal{E}}^{-1}(\boldsymbol{\theta})\boldsymbol{\mathcal{B}}(\boldsymbol{\theta})[1+z]$ with respect to $\boldsymbol{\theta}_i$ are

$$\frac{\partial \boldsymbol{A}(\boldsymbol{\theta})}{\partial \boldsymbol{\theta}_i} = -\boldsymbol{\mathcal{E}}^{-1}(\boldsymbol{\theta})\frac{\partial \boldsymbol{\mathcal{E}}(\boldsymbol{\theta})}{\partial \boldsymbol{\theta}_i}\boldsymbol{\mathcal{E}}^{-1}(\boldsymbol{\theta})\boldsymbol{\mathcal{A}}(\boldsymbol{\theta}) + \boldsymbol{\mathcal{E}}^{-1}(\boldsymbol{\theta})\frac{\partial \boldsymbol{\mathcal{A}}(\boldsymbol{\theta})}{\partial \boldsymbol{\theta}_i}, \tag{C3}$$

$$\frac{\partial \boldsymbol{B}(\boldsymbol{\theta})}{\partial \boldsymbol{\theta}_i} = \left(-\boldsymbol{\mathcal{E}}^{-1}(\boldsymbol{\theta})\frac{\partial \boldsymbol{\mathcal{E}}(\boldsymbol{\theta})}{\partial \boldsymbol{\theta}_i}\boldsymbol{\mathcal{E}}^{-1}(\boldsymbol{\theta})\boldsymbol{\mathcal{B}}(\boldsymbol{\theta}) + \boldsymbol{\mathcal{E}}^{-1}(\boldsymbol{\theta})\frac{\partial \boldsymbol{\mathcal{B}}(\boldsymbol{\theta})}{\partial \boldsymbol{\theta}_i}\right)[1+z]. \tag{C4}$$

Substitution of Equations (C3) and (C4) into Equation (C2) finally gives

$$\begin{aligned}\frac{\partial G_{i_u,i_y}(z,\boldsymbol{\theta})}{\partial \boldsymbol{\theta}_i} &= \boldsymbol{C}\left[z\boldsymbol{I} - \boldsymbol{A}(\boldsymbol{\theta})\right]^{-1}\boldsymbol{\mathcal{E}}^{-1}(\boldsymbol{\theta})(1+z) \\ &\times\left\{\left(\frac{\partial \boldsymbol{\mathcal{B}}(\boldsymbol{\theta})}{\partial \boldsymbol{\theta}_i} + \frac{\partial \boldsymbol{\mathcal{A}}(\boldsymbol{\theta})}{\partial \boldsymbol{\theta}_i}\left[z\boldsymbol{I} - \boldsymbol{A}(\boldsymbol{\theta})\right]^{-1}\boldsymbol{\mathcal{E}}^{-1}(\boldsymbol{\theta})\boldsymbol{\mathcal{B}}(\boldsymbol{\theta})\right)\right. \\ &- \frac{\partial \boldsymbol{\mathcal{E}}(\boldsymbol{\theta})}{\partial \boldsymbol{\theta}_i}\boldsymbol{\mathcal{E}}^{-1}(\boldsymbol{\theta})(\boldsymbol{\mathcal{B}}(\boldsymbol{\theta}) + \boldsymbol{\mathcal{A}}(\boldsymbol{\theta})\left[z\boldsymbol{I} - \boldsymbol{A}(\boldsymbol{\theta})\right]^{-1} \\ &\left.\times\,\boldsymbol{\mathcal{E}}^{-1}(\boldsymbol{\theta})\boldsymbol{\mathcal{B}}(\boldsymbol{\theta}))\right\}\end{aligned} \tag{C5}$$

In this equation, the derivatives can be found analytically using Equations (18) and (19). To evaluate this equation at $\boldsymbol{\theta} = \boldsymbol{\theta}_0$ for all parameters $\boldsymbol{\theta}_i \in \boldsymbol{\theta}$, it is most efficient to follow these steps:

(1) Calculate all terms independent of z in Equation (C5) for $\boldsymbol{\theta} = \boldsymbol{\theta}_0$ once and store these.
(2) Evaluate for $\boldsymbol{\theta}_i$ the expression (C5) at frequency ω by substituting $z = \exp(i\omega T_s)$
(3) Repeat step (2) for all other $i = 1, \ldots, \dim(\boldsymbol{\theta})$.
(4) Repeat steps (2) and (3) until the gradient is computed for all required frequencies ω.

Combining the derivatives of each element in the parameter vector then gives the gradient.